Edge Flux Intensity Functions in Polyhedral Domains and their Extraction by a Quasidual Function Method

Netta OMER[1], Zohar YOSIBASH[1*], Martin COSTABEL[2] & Monique DAUGE[2]

April 19, 2004

[1] Dept. of Mechanical Engineering., Ben-Gurion University of the Negev,
Beer-Sheva, 84105, ISRAEL
[2] UMR CNRS 6625 – IRMAR, Université de Rennes 1 – Campus de Beaulieu,
35042 Rennes Cedex, FRANCE

Abstract

The asymptotics of solutions to scalar second order elliptic boundary value problems in three-dimensional polyhedral domains in the vicinity of an edge is provided in an explicit form. It involves a family of eigen-functions with their shadows, and the associated edge flux intensity functions (EFIFs), which are functions along the edges. Utilizing the explicit structure of the solution in the vicinity of the edge we present a new method for the extraction of the EFIFs called *quasidual function method*. It can be interpreted as an extension of the dual function contour integral method in 2-D domains, and involves the computation of a surface integral $J[R]$ along a cylindrical surface of radius R away from the edge as presented in a general framework in [8]. The surface integral $J[R]$ utilizes special constructed extraction polynomials together with the dual eigen-functions for extracting EFIFs.

This accurate and efficient method provides a polynomial approximation of the EFIF along the edge whose order is adaptively increased so to approximate the exact EFIF. It is implemented as a post-solution operation in conjunction with the p-version finite element method. Numerical realization of some of the anticipated properties of the $J[R]$ are provided, and it is used for extracting EFIFs associated with different scalar elliptic equations in 3-D domains, including domains having edge and vertex singularities. The numerical examples demonstrate the efficiency, robustness and high accuracy of the proposed quasi-dual function method, hence its potential extension to elasticity problems.

1. Introduction.

1.a The framework

The solutions of elliptic boundary value problems, for example those arising in heat transfer and elasticity, when posed and solved in non-smooth domains like polygons and polyhedra, have non-smooth parts. These are described in terms of special singular functions depending on the geometry and the differential operators on one hand, and of unknown coefficients depending on the given right hand side and boundary conditions on the other hand.

Concerning the singular functions, they are extensively covered in the literature. In many cases like corners in two dimensions or edges in three dimensions, they can be written analytically (see

*Corresponding author

for example [12, 3]) or semi-analytically [7]. In other cases like polyhedral corners, there exist well-known numerical methods for their computation (see for example [2, 17]).

Scalar elliptic boundary value problems in three-dimensional domains (as the heat transfer problem in engineering practice), contain singular solutions along each of the domain's *edges*. Each such singularity along an edge E is characterized:

- by an *exponent* α which belongs to a discrete set $\{\alpha_i,\ i \in \mathbb{N}\}$ of eigen-values depending only on the geometry and the operator, and which determines the level of non-smoothness of the singularity. Any *eigen-value* α_i is computed by solving a 2-D problem.
- by an *eigen-function* $\varphi_0^{(\alpha)}(\theta)$ which depends on the geometry of the domain and the operator. These eigen-functions are computed by solving a set of 2-D problems.
- by a *function* along the edge E, denoted by $A^{(\alpha)}(x_3)$ (x_3 is a coordinate along the edge) and called "Edge Flux Intensity Function" (EFIF) which determines the "amount of energy" residing in each singularity.

The complete expansion of the solution in the vicinity of an edge is described in [8] as a combination of eigen-functions and their "shadows". These shadows are new functions appearing in 3-D domains, having no counterparts in 2-D domains as far as homogeneous operators with constant coefficients are concerned. There exists also a sequence of dual eigen-functions and their dual shadows. Their explicit knowledge is required in our quasi-dual function method for the computation of the EFIFs.

From the engineering perspective the EFIFs $A^{(\alpha)}(x_3)$ when $\alpha < 1$ are of major importance because these are correlated to failure initiation. In many situations $\alpha < 1$ when the opening at the edge is non-convex. For example α can be equal to $\frac{1}{2}$ in the presence of cracks.

This work is motivated by the need to compute generalized stress intensity functions along edges for elasticity problems in 3-D domains. These are of significant engineering importance in cracked and V-notched structures, in which the stress intensity functions may (and often do) vary along the crack front. Present methods for extracting edge stress intensity functions (ESIFs) in cracked 3-D domains, as the J-integral [5, 14, 16] for example, are limited to plane-strain/stress assumptions, provide the point-wise value of the ESIF at a given point along the edge, and require the computation of an area integral containing the singular point (thus may include large errors when used in conjunction with numerical methods). Furthermore, the point-wise path-area-independent J-integral in 3-D domains is not exactly related to the mode-I, II and III stress intensity functions when these vary along the edge. Other methods, as the B- and H-integrals [15], suffer from the same difficulties as these mentioned above.

Our method as initiated in [8], uses analytic forms of the asymptotic expansion of the displacements and stresses in the vicinity of an edge, and it leads to an algorithm for computing the ESIFs (provided as a *function* along the edge and not only pointwise values). In order to explain the ideas of the implementation of the method and to test its efficiency, we first consider general scalar second order elliptic problems, homogeneous with constant coefficients. These are simpler elliptic problems that allow more transparent analytic computations, although they invoke all necessary characteristics of the elasticity system. Thus, the characteristics of the solution can be more easily addressed and the new method for computing the EFIFs can be demonstrated. The next step will be the computation of ESIFs in isotropic elasticity problems.

1.b The method

Using the eigen-functions and their shadows, a new functional $J[R]$ is introduced (following [8]), which can be viewed as an extension of the 2-D contour integral (see e.g. [4]) to 3-D domains.

This new functional, which is a surface integral along a cylindrical surface, enables us to present the edge flux intensity function explicitly as a function of x_3 (the coordinate along the edge). The method presented is implemented as a post-processing step in a p-version finite element code and the numerical performance is documented on several example problems. Using the $J[R]$ functional, and newly constructed extraction polynomials, we extract the EFIFs in the vicinity of any edge (including crack front) in any polyhedron. This method is easily extendable to problems of 3-D elasticity and is the first method to *provide the functional representation of the EFIFs along* x_3 (as opposed to other methods providing pointwise values of the EFIFs along the edge) and is very accurate, efficient and robust. Most importantly, *the method is adaptive*, providing a better polynomial representation of the EFIF as the special hierarchical family of extraction polynomials is increased. Cases where the EFIF has very large gradients and where edges approach vertices are considered, and we show the method's robustness and accuracy for these cases as well.

This paper is organized as follows:

- We start with notations, defining the domain of interest and the different elliptic operators we consider.
- We describe the asymptotic expansion of the solution in the neighborhood of an edge in terms of eigen-functions, their shadows, and the structure of the EFIFs. The dual eigen-functions, and their shadows, which are associated with the primal eigen-functions are addressed as well.
- The $J[R]$ integral is then introduced, and the main theorem for extracting the EFIFs is quoted (the proof can be found in [8]). This integral requires the construction of extracting polynomials, denoted by $B(x_3)$, and the data on a surface of a cylinder of radius R with the edge as its axis. A short explanation on its application in conjunction with the finite element method is given. We then describe the various problems chosen as test cases for our computations (for which we provide in Appendices A and B the explicit formulas for the eigen-functions, duals and shadows). Numerical experimentations are performed to demonstrate that the computed $J[R]$'s indeed provide the anticipated trends expected by the theorem.
- Subsequently, a hierarchical family of extraction polynomials is constructed. The hierarchical family of extraction polynomials is used in many numerical tests to extract the EFIFs.
- Finally, we present two numerical examples where the EFIF has large gradients, and where the edge approaches a vertex. These examples demonstrate the robustness of the method in handling realistic geometries in engineering practice.

2. The Model Domain and the Scalar Elliptic Problem.

As a model, we choose a domain Ω such that only one straight edge E is present. The domain is generated as the product $\Omega = G \times I$ where I is the interval $[-1, 1]$, and G is a plane bounded sector of opening $\omega \in (0, 2\pi]$ and radius 1 (the case of a crack, $\omega = 2\pi$, is included), as shown in Figure 1. Although any radius or interval I can be chosen, these simplified numbers have been chosen for simplicity of presentation. In §7. we consider a less elementary example.

The variables in G and I are (x_1, x_2) and x_3 respectively, and the coordinates (x_1, x_2, x_3) are denoted by $\boldsymbol{x}$. Let (r, θ) be the polar coordinates centered at the vertex of G so that G coincides with $\{(x_1, x_2) \in \mathbb{R}^2 \mid r \in (0, 1),\ \theta \in (0, \omega)\}$. The *edge* E of interest is the set

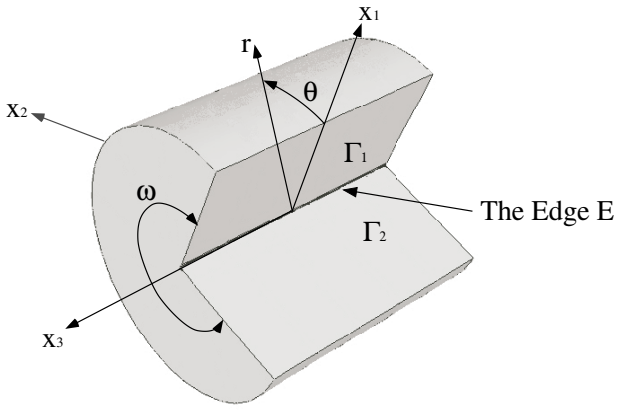

Figure 1. *Model domain of interest* Ω .

$\{\boldsymbol{x} \in \mathbb{R}^3 \mid r = 0,\ x_3 \in I\}$. The two flat planes that intersect at the edge E are denoted by Γ_1 and Γ_2 . For any R , $0 < R < 1$, the cylindrical surface Γ_R is defined as follows:

$$\Gamma_R := \big\{\boldsymbol{x} \in \mathbb{R}^3 \mid r = R,\ \theta \in (0, \omega),\ x_3 \in I\big\}. \tag{2.1}$$

Remark 2.1 *The methods presented in the paper are restricted to geometries where the edges are straight lines and the angle* ω *is fixed along* x_3 .

The considered operator is an elliptic second order partial differential operator L with constant real coefficients (k_{ij}) of the form:

$$L = \sum_{i=1}^{3}\sum_{j=1}^{3} k_{ij}\partial_i\partial_j \quad \text{with} \quad \partial_1 = \frac{\partial}{\partial x_1},\ \partial_2 = \frac{\partial}{\partial x_2},\ \partial_3 = \frac{\partial}{\partial x_3}\,,$$

where $k_{ij} = k_{ji}$ form a symmetric matrix 3×3 (for heat transfer problems these represent the heat conduction coefficients). The k_{ij} 's have to satisfy the ellipticity condition, and without loss of generality k_{33} is set as $k_{33} = 1$. Denoting the solution by $\tau(\boldsymbol{x})$, we consider the Dirichlet problem on Ω

$$\begin{cases} L(\tau) &= 0 \quad \text{in} \quad \Omega \\ \tau &= g \quad \text{on} \quad \partial\Omega, \end{cases} \tag{2.2}$$

where g is the trace of a given function belonging to $H^1(\Omega)$. We assume that the Dirichlet boundary conditions are homogeneous on Γ_1 and Γ_2 , i.e.:

$$g(r, 0, x_3) = g(r, \omega, x_3) = 0. \tag{2.3}$$

Note that all methods presented herein carry over to Neumann or mixed homogenous boundary conditions also.

For demonstration purposes three specific operators are considered: the Laplace operator, $k_{ij} = \delta_{ij}$, a general operator with $k_{11} = 5, k_{22} = 4$, $k_{12} = -4$ and $k_{13} = k_{23} = 0$ and a general operator having also mixed derivatives in the x_3 direction with $k_{11} = k_{22} = 1$, $k_{13} = -0.5$

and $k_{12} = k_{23} = 0$. Two domains are considered as benchmark domains, namely one having $\omega = 3\pi/2$ and the other one is a cracked domain, $\omega = 2\pi$. Combining the two different domains and three different operators we define five specific Cases according to Table 1.

Case #	ω	The Operator					
		k_{11}	k_{22}	k_{33}	k_{12}	k_{13}	k_{23}
Case 1	$3\pi/2$	1	1	1	0	0	0
Case 2	$3\pi/2$	5	4	1	-4	0	0
Case 3	2π	1	1	1	0	0	0
Case 4	2π	5	4	1	-4	0	0
Case 5	2π	1	1	1	0	-0.5	0

Table 1. *Notation of the various Cases considered as model problems*

3. The Singular Solutions in the Vicinity of the Edge.

The asymptotic representation of the exact solution τ for the problem (2.2) in the neighborhood of the edge E relies on splitting the operator L into three parts (see [13, 9, 6]):

$$L = M_0(\partial_1, \partial_2) + M_1(\partial_1, \partial_2)\partial_3 + M_2\partial_3^2, \tag{3.1}$$

with M_0 a second order operator, M_1 a first order operator and M_2 a constant. This splitting allows to consider for τ an Ansatz of the form:

$$\widetilde{\tau} = \sum_{j\geq 0} \partial_3^j A(x_3)\, \Phi_j(x_1, x_2), \tag{3.2}$$

which should solve the homogeneous equation $L(\widetilde{\tau}) = 0$ together with the lateral boundary conditions $\widetilde{\tau}(r, 0, x_3) = \widetilde{\tau}(r, \omega, x_3) = 0$, *cf* (2.3). After inserting (3.2), the equation $L(\widetilde{\tau}) = 0$ becomes:

$$\sum_{j\geq 0} \partial_3^j A(x_3)\, M_0\Phi_j + \sum_{j\geq 0} \partial_3^{j+1} A(x_3)\, M_1\Phi_j + \sum_{j\geq 0} \partial_3^{j+2} A(x_3)\, M_2\Phi_j = 0 \tag{3.3}$$

and after rearranging:

$$A(x_3)M_0\Phi_0 + \partial_3^1 A(x_3)(M_0\Phi_1 + M_1\Phi_0) + \\ + \sum_{j\geq 2} \partial_3^j A(x_3)(M_0\Phi_j + M_1\Phi_{j-1} + M_2\Phi_{j-2}) = 0. \tag{3.4}$$

We want that equation (3.4) holds for any smooth function $A(x_3)$. Thus, the functions Φ_j have to satisfy the three equations below:

$$\begin{cases} M_0\Phi_0 = 0 \\ M_0\Phi_1 + M_1\Phi_0 = 0 & (x_1, x_2) \in G \\ M_0\Phi_j + M_1\Phi_{j-1} + M_2\Phi_{j-2} = 0, \quad j \geq 2 \end{cases} \tag{3.5}$$

accompanied by the homogeneous Dirichlet boundary conditions on the two faces $\theta = 0, \omega$:

$$\Phi_j(r,0) = \Phi_j(r,\omega) = 0. \tag{3.6}$$

The first partial differential equation in (3.5) with (3.6) has solutions Φ_0 of the form

$$\Phi_0 = r^{\alpha}\varphi_0(\theta)$$

with α in a discrete set $\{\alpha_i,\ i \in \mathbb{N}\}$ of positive numbers. These solutions are refered to as the two-dimensional *primal singular functions*. They are nothing but the singular solutions associated with the eigen-value α of the boundary value problem generated over the 2-D domain G.

The second PDE in (3.5) with homogeneous Dirichlet boundary conditions (3.6) generates the function Φ_1 which depends on Φ_0 and is of the form: $\Phi_1 = r^{\alpha+1}\varphi_1(\theta)$. Finally, the solutions of the third equation of (3.5) with conditions (3.6) form the sequence Φ_j :

$$\Phi_j = r^{\alpha+j}\varphi_j(\theta). \tag{3.7}$$

The Φ_j , $j \geq 1$, are called the *"shadow" functions* associated with the leading function Φ_0 . To each value α_i of α corresponds a sequence (Φ_j) which we denote from now on by $(\Phi_j^{(\alpha_i)})$:

$$\Phi_j^{(\alpha_i)} = r^{\alpha_i+j}\varphi_j^{(\alpha_i)}(\theta) \quad j = 0, 1, \ldots \tag{3.8}$$

Thus, for each eigen-value α_i and each coefficient $A^{(\alpha_i)}$ (smooth enough) the 3-D function:

$$\widetilde{\tau} = \sum_{j\geq 0} \partial_3^j A^{(\alpha_i)}(x_3)\, r^{\alpha_i+j}\varphi_j^{(\alpha_i)}(\theta) \tag{3.9}$$

solves the homogeneous equation $L(\widetilde{\tau}) = 0$ together with the lateral homogeneous Dirichlet conditions. It can be shown that the overall solution τ of problem (2.2) can be expanded as:

$$\tau = \sum_{i\geq 1}\sum_{j\geq 0} \partial_3^j A^{(\alpha_i)}(x_3)\, r^{\alpha_i+j}\varphi_j^{(\alpha_i)}(\theta), \qquad \text{as} \quad r \to 0, \tag{3.10}$$

where $A^{(\alpha_i)}(x_3)$ is the Edge Flux Intensity Function (EFIF) associated with the i^{th} eigen-value.

Solutions of (3.5)-(3.6) associated with the *negative eigen-values* are called the *dual singular solutions*, and are denoted by Ψ . Since the operator L is self-adjoint, for any α_i the number $-\alpha_i$ is also an eigen-value and there exists $\psi_0^{(\alpha_i)}$ such that $r^{-\alpha_i}\psi_0^{(\alpha_i)}(\theta)$ solves the first equation of (3.5). For normalization reasons, we set, for some real coefficient $c_0^{(\alpha_i)}$:

$$\Psi_0^{(\alpha_i)} = c_0^{(\alpha_i)} r^{-\alpha_i}\psi_0^{(\alpha_i)}(\theta) \tag{3.11}$$

where $\Psi_0^{(\alpha_i)}$ is the dual leading eigen-solution and

$$\Psi_j^{(\alpha_i)} = c_0^{(\alpha_i)} r^{-\alpha_i+j}\psi_j^{(\alpha_i)}(\theta) \tag{3.12}$$

are the shadow dual eigen-solutions. Computation of primal and dual eigen-functions for Cases 1-4 is provided in Appendix A, and for Case 5 in Appendix B. Theoretical details and rigorous mathematical formulation is provided in [8].

Remark 3.1 *Operators for which* $M_1 = 0$ *imply that the* Φ_j *and* Ψ_j *of odd rank are zero:* $\Phi_j^{(\alpha_i)} = \Psi_j^{(\alpha_i)} = 0$, $j = 1, 3, 5, \ldots$

4. The Extraction Method - The $J[R]$ Integral.

For each eigen-value α_i , a set of *quasidual* singular functions $K_m^{(\alpha_i)}[B_m]$ are constructed where m is a natural integer called the *order* of the quasidual function, and $B_m(x_3)$ is a function (we choose it to be a polynomial) called *extraction polynomial*.

$$K_m^{(\alpha_i)}[B_m] \stackrel{\text{def}}{=} \sum_{j=0}^{m} \partial_3^j B_m(x_3)\, \Psi_j^{(\alpha_i)}. \tag{4.1}$$

By using the quasidual functions, one can extract a scalar product of $A^{(\alpha_i)}(x_3)$ with $B_m(x_3)$ on E . This is accomplished with the help of the *anti-symmetric* boundary integral $J[R]$, over the surface Γ_R (2.1). We define $J[R](u,v)$ to be:

$$J[R](u,v) \stackrel{\text{def}}{=} \int_{\Gamma_R} (Tu\cdot v - u\cdot Tv)\, dS = \int_I \int_0^w (Tu\cdot v - u\cdot Tv)|_{r=R}\, R\, d\theta\, dx_3 \tag{4.2}$$

where $I \equiv E$ (the edge) along x_3 axis (Figure 1). T is the radial Neumann trace operator related to the operator L :

$$T \stackrel{\text{def}}{=} \left\{ \begin{pmatrix} k_{11} & k_{12} & k_{13} \\ k_{21} & k_{22} & k_{23} \\ k_{31} & k_{32} & 1 \end{pmatrix} \begin{pmatrix} \partial_1 \\ \partial_2 \\ \partial_3 \end{pmatrix} \right\}^T \begin{pmatrix} \cos\theta \\ \sin\theta \\ 0 \end{pmatrix}. \tag{4.3}$$

With the above definition we have the following theorem [8]:

Theorem 4.1 *Take* $B_m(x_3)$ *such that*

$$\partial_3^j B_m(x_3) = 0 \quad \textit{for} \quad j = 0, ..., m-1 \quad \textit{on } \partial I \tag{4.4}$$

then, if the EFIFs $A^{(\alpha_i)}$ *in the expansion* (3.10) *are smooth enough:*

$$J[R](\tau, K_m^{(\alpha_i)}[B_m]) = \int_I A^{(\alpha_i)}(x_3)\, B_m(x_3)\, dx_3 + \mathcal{O}(R^{\alpha_1-\alpha_i+m+1}), \quad \textit{as} \quad R\to 0. \tag{4.5}$$

Here α_1 *is the smallest of the eigen-values* α_i , $i \in \mathbb{N}$.

Theorem 4.1 allows a precise determination of $\int_I A^{(\alpha_i)}(x_3)\, B_m(x_3)\, dx_3$ by computing (4.4) for two or three R values and using Richardson's extrapolation as $R \to 0$.

Remark 4.2 *For the first EFIF* $A^{(\alpha_1)}$ *, we obtain the highest convergence rate* $\mathcal{O}(R^{m+1})$ *. If, moreover, the* Φ_j *and* Ψ_j *of odd rank are zero, cf Remark 3.1, there holds the following improvement of Theorem 4.1: For any* even *integer* m *, condition* (4.4) *implies that the asymptotic equality* (4.5) *holds modulo a remainder in* $\mathcal{O}(R^{m+2})$ *instead of* $\mathcal{O}(R^{m+1})$ *.*

4.a The quasidual extraction functions.

To confirm that the numerical examples provide the results predicted by Theorem 4.1 we consider the following options of the quasidual extraction functions:

$$K_0^{(\alpha_1)} = B_0(x_3)\Psi_0^{(\alpha_1)}(r,\theta)$$
$$K_1^{(\alpha_1)} = B_1(x_3)\Psi_0^{(\alpha_1)}(r,\theta) + \partial_3 B_1(x_3)\Psi_1^{(\alpha_1)}(r,\theta)$$
$$K_2^{(\alpha_1)} = B_2(x_3)\Psi_0^{(\alpha_1)}(r,\theta) + \partial_3 B_2(x_3)\Psi_1^{(\alpha_1)}(r,\theta) + \partial_3^2 B_2(x_3)\Psi_2^{(\alpha_1)}(r,\theta)$$
$$K_3^{(\alpha_1)} = B_3(x_3)\Psi_0^{(\alpha_1)}(r,\theta) + \partial_3 B_3(x_3)\Psi_1^{(\alpha_1)}(r,\theta) + \partial_3^2 B_3(x_3)\Psi_2^{(\alpha_1)}(r,\theta) + \partial_3^3 B_3(x_3)\Psi_3^{(\alpha_1)}(r,\theta)$$

According to Theorem 4.1, the difference between the integral $J[R](\tau, K_m^{(\alpha_i)}[B_m])$ and the moment $\int_I A^{(\alpha_i)}(x_3)\, B_m(x_3)\, dx_3$ should be of the order of R^{m+1}, which is the convergence rate with respect to R. To obtain the "right" convergence rate, the following conditions should be satisfied for the extraction polynomials B_0, B_1, B_2 and B_3 according to condition (4.4):

$$B_0: \quad \text{No condition required.} \tag{4.6}$$
$$B_1: \quad B_1(+1) = B_1(-1) = 0 \tag{4.7}$$
$$B_2: \quad B_2(+1) = B_2(-1) = \partial_3 B_2(+1) = \partial_3 B_2(-1) = 0 \tag{4.8}$$
$$B_3: \quad B_3(+1) = B_3(-1) = \partial_3 B_3(+1) = \partial_3 B_3(-1) = \partial_3^2 B_3(+1) = \partial_3^2 B_3(-1) = 0. \tag{4.9}$$

Since B_0 does not have to satisfy any condition, we choose $B_0(x_3) = 1$. We further choose $B_1(x_3) = x_3^2 - 1$, $B_2(x_3) = (x_3^2-1)^2$ and $B_3(x_3) = (x_3^2-1)^3$ which satisfy (4.7), (4.8) and (4.9) respectively.

The exact solution τ being unknown in general, we use instead a finite element approximation $\tau_{\rm FE}$ and the integral (4.2) is performed numerically using a Gaussian quadrature of order n_G:

$$J[R](\tau, K_m^{(\alpha_i)}[B_m]) = \sum_{k=1}^{n_G}\sum_{\ell=1}^{n_G} \frac{\omega}{2}\, w_k w_\ell \left(T\tau_{\rm FE}\cdot K_m^{(\alpha_i)}[B_m] - \tau_{\rm FE}\cdot TK_m^{(\alpha_i)}[B_m]\right)_{\xi_k,\eta_\ell} \tag{4.10}$$

where w_k are the weights and ξ_k and η_ℓ are the abscissas of the Gaussian quadrature. The Neumann trace operator, T, operates on both τ and $K_m^{(\alpha_i)}[B_m]$. For $T\tau$ we use the numerical approximations $T\tau_{\rm FE}$ computed by finite elements. We extract in the post-solution phase of the FE analysis $\tau_{\rm FE}$, $\partial_1\tau_{\rm FE}$, $\partial_2\tau_{\rm FE}$, and $\partial_3\tau_{\rm FE}$ (note that such extractions are possible without problems thanks to the p-version of FEM) whereas $TK_m^{(\alpha_i)}[B_m]$ is computed analytically. These values are evaluated at the specific Gaussian points when the integral is computed numerically.

The numerical errors associated with the numerical integration and with replacing the exact solution by the finite element solution are negligible, as shown for one example problem in Appendix C.

4.b Analytical Solutions for Validating the $J[R]$ Integral Method

We generate herein analytical solutions against which our numerical experimentations are compared. The exact solution associated with the i-th eigen-pair, $\tau_{\rm ex}^{(\alpha_i)}$ is:

$$\tau_{\rm ex}^{(\alpha_i)} = \sum_{j\geq 0} \partial_3^j A^{(\alpha_i)}(x_3)\, \Phi_j^{(\alpha_i)}(r,\theta) \tag{4.11}$$

So if $A^{(\alpha_i)}(x_3)$ is a polynomial of order N, i.e. $A^{(\alpha_i)}(x_3) = a_0 + a_1 x_3 + \cdots + a_N x_3^N$ then (4.11) has a finite number of terms in the sum, because the $N+1$ and higher derivatives are zero. Thus, (4.11) becomes:

$$\tau_{\text{ex}}^{(\alpha_i)} = \sum_{j=0}^{N} \partial_3^j A^{(\alpha_i)}(x_3)\, \Phi_j^{(\alpha_i)}(r,\theta). \tag{4.12}$$

Recall that, by the mere construction of the $\Phi_j^{(\alpha_i)}$, there holds $L\tau_{\text{ex}}^{(\alpha_i)} = 0$. If we specify over the entire boundary $\partial\Omega$ the Dirichlet boundary condition g as the trace of (4.12), the solution τ of problem (2.2) coincides with (4.12) at any point $\boldsymbol{x} \equiv (r,\theta,x_3)$.

We coose two examples of boundary conditions, each having a different N. The first BC, which is denoted by (BC_2) is the one for which we take $N=2$ and

$$A^{(\alpha_1)}(x_3) = 1 + x_3 + x_3^2 \tag{4.13}$$

i.e., $a_0 = a_1 = a_2 = 1$. This means that we prescribe the Dirichlet condition on $\partial\Omega$:

$$(\text{BC}_2) \qquad \tau_{\text{ex}}^{(\alpha_1)}\big|_{\partial\Omega} = (1 + x_3 + x_3^2)\Phi_0^{(\alpha_1)}(r,\theta) + (1+2x_3)\Phi_1^{(\alpha_1)}(r,\theta) + 2\Phi_2^{(\alpha_1)}(r,\theta).$$

The second boundary condition which we consider is for $N=4$, is denoted by (BC_4) for which we take

$$A^{(\alpha_1)}(x_3) = 5 + 4x_3 + 9x_3^2 + 3x_3^3 + x_3^4 \tag{4.14}$$

i.e. $a_0 = 5$, $a_1 = 4$, $a_2 = 9$, $a_3 = 3$ and $a_4 = 1$. This means that we have the Dirichlet condition:

$$\begin{aligned}(\text{BC}_4) \qquad \tau_{\text{ex}}^{(\alpha_1)}|_{\partial\Omega} &= (5 + 4x_3 + 9x_3^2 + 3x_3^3 + x_3^4)\,\Phi_0^{(\alpha_1)}(r,\theta) \\ &+ (4 + 18x_3 + 9x_3^2 + 4x_3^3)\,\Phi_1^{(\alpha_1)}(r,\theta) \\ &+ (18 + 18x_3 + 12x_3^2)\,\Phi_2^{(\alpha_1)}(r,\theta) \\ &+ (18 + 24x_3)\,\Phi_3^{(\alpha_1)}(r,\theta) + 24\Phi_4^{(\alpha_1)}(r,\theta).\end{aligned}$$

By the uniqueness of solutions, the solution of problem (2.2) with the boundary condition (BC_2) and (BC_4) coincides with $\tau_{\text{ex}}^{(\alpha_1)}$ for the choice (4.13) and (4.14) of $A^{(\alpha_1)}$, respectively. This means that our exact solution contains only one edge singularity (and no vertex singularities).

The domains have been discretized by using a p-FEM mesh, with geometrical progression towards the singular edge with a factor of 0.15, having 4 layers of elements. In the x_3 direction, a uniform discretization using 5 elements has been adopted. In Figure 2 we present the meshes used for opening angles of $\omega = 3\pi/2$ and $\omega = 2\pi$ (crack).

4.c Numerical Tests Using $K_0^{(\alpha_1)}$ for Cases 1 to 4

When using the quasidual function $K_0^{(\alpha_1)}$ with any chosen $B_0(x_3)$, according to Theorem 4.1 the convergence of $J[R]$ to $J[0]$ should be $\mathcal{O}(R^2)$ for Cases 1-4 (for which $\Phi_1 = \Psi_1 = 0$, *cf* Remark 4.2). We perform numerical tests for Cases 1-4 taking the boundary condition (BC_2) and computing $J[R]$ at different values of R.

According to equation (4.5), we have:

$$J[0] = \lim_{R\to 0} J[R](\tau, K_0^{(\alpha_i)}[B_0]) = \int_I A^{(\alpha_i)}(x_3) B_0(x_3) dx_3 \overset{\text{def}}{=} J_{\text{ex}}. \tag{4.15}$$

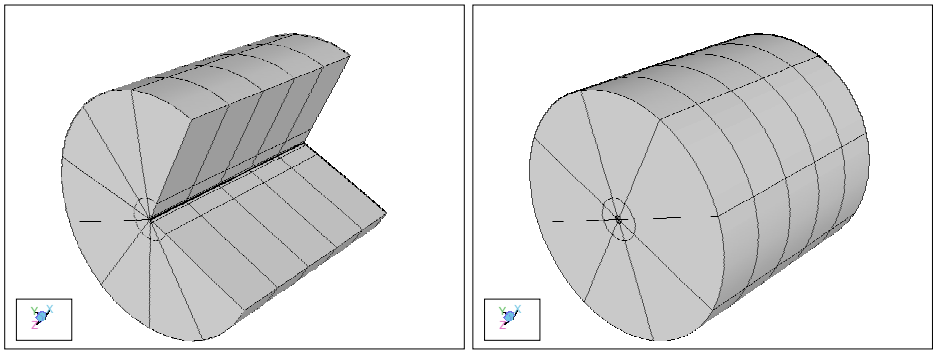

Figure 2. *The p-FEM models.*

With the fixed extraction polynomial $B_0(x_3) = 1$, we find for $A(x_3) = 1 + x_3 + x_3^2$ and $K_0^{(\alpha_1)}$:

$$J_{\text{ex}} = \int_{-1}^{1} (1 + x_3 + x_3^2) \cdot 1 \, dx_3 = \frac{8}{3}.$$

We have computed $J[R]$ according to formula (4.10) with 10 integration points for the quadrature in both θ and x_3 directions and with the degree $p = 6$ in the finite element analysis. It was found out that taking 32 integration points and $p = 8$ does not improve the results considerably.

We summarize the results in Table 2, and plot in Figure 3 $\log(J_{\text{ex}} - J[R])$ vis. $\log(R)$, which yields the numerical convergence rate.

	Case 1	Case 2	Case 3	Case 4
$R = 0.9$	0.544627	0.857214	0.393094	0.704199
$R = 0.8$	0.639754	0.886932	0.519466	0.764039
$R = 0.7$	0.724304	0.913497	0.632346	0.819377
$R = 0.6$	0.797786	0.936658	0.730629	0.868391
$R = 0.5$	0.859434	0.955926	0.812665	0.907785
$R = 0.4$	0.909614	0.971456	0.879250	0.939072
$R = 0.3$	0.949535	0.984096	0.932802	0.967113
$R = 0.2$	0.977493	0.992844	0.970071	0.983999
$R = 0.1$	0.994679	0.998349	0.993188	0.996935

Table 2. *Values of $J[R]/J_{\text{ex}}$ for (BC_2), using $K_0^{(\alpha_1)}$ and $B_0(x_3) = 1$.*

It is easily visible in Figure 3 that the convergence rate in Cases 1-4 is $\mathcal{O}(R^2)$ as expected (on each graph the line of slope 2 passing through the first point of the graph has been plotted).

4.d Numerical Tests using $K_0^{(\alpha_1)}$ to $K_3^{(\alpha_1)}$ for Case 5

Taking $K_0^{(\alpha_1)}$ up to $K_m^{(\alpha_1)}$, where highest m is 3, and with extraction polynomials $B_m(x_3)$ that satisfy (4.8), the convergence of $J[R]$ to the exact value should be $\mathcal{O}(R^{m+1})$ for Case 5.

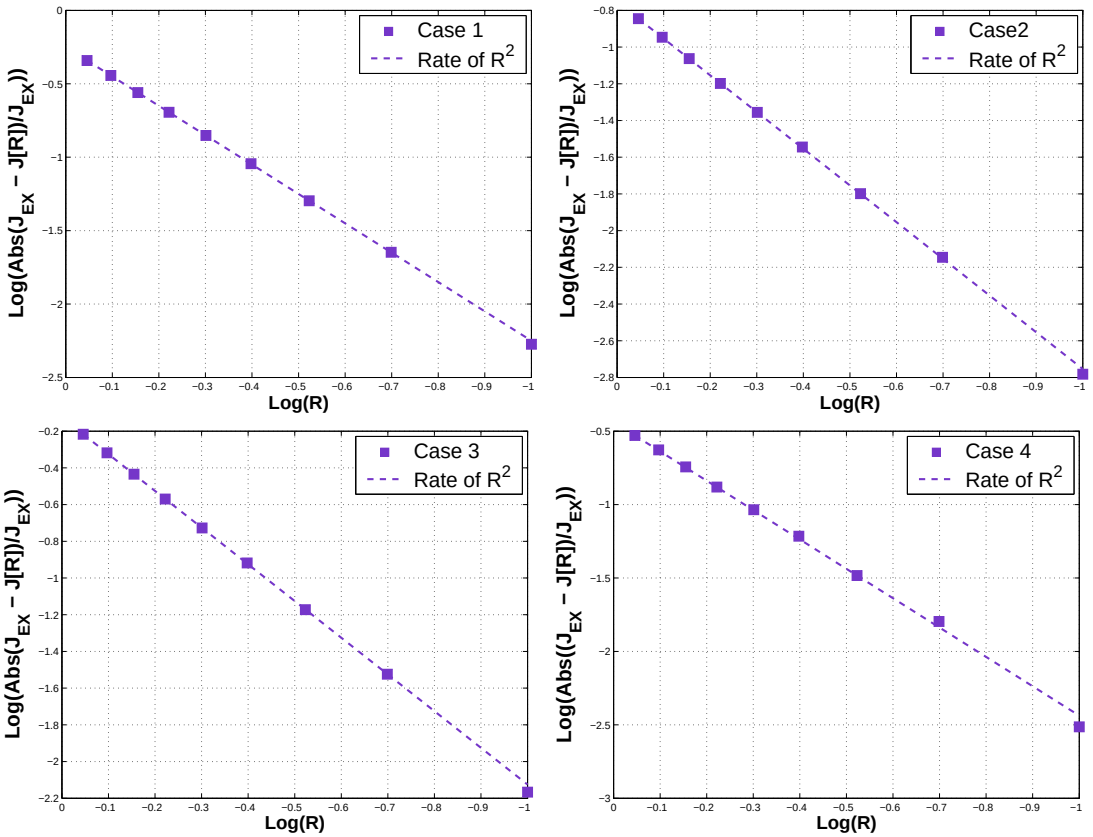

Figure 3. *Convergence rates of* $J[R]$ *for* (BC_2), *with* $K_0^{(\alpha_1)}$ *and* $B_0 = 1$.

$B_m(x_3)$ J_{ex}	$K_0^{(\alpha_1)}$ 1 $8/3$	$K_1^{(\alpha_1)}$ x_3^2-1 $-8/5$	$K_2^{(\alpha_1)}$ $(x_3^2-1)^2$ $128/105$	$K_3^{(\alpha_1)}$ $(x_3^2-1)^3$ $-64/63$
$R = 0.9$	0.452184	0.170991	1.066583	1.291903
$R = 0.8$	0.549460	0.334150	1.093614	1.161184
$R = 0.7$	0.638916	0.483345	1.094800	1.082724
$R = 0.6$	0.719399	0.616099	1.080202	1.038806
$R = 0.5$	0.789221	0.729563	1.057599	1.015371
$R = 0.4$	0.849224	0.823832	1.034622	1.004237
$R = 0.3$	0.901877	0.900601	1.017906	1.001634
$R = 0.2$	0.943800	0.955126	1.005847	1.000079
$R = 0.1$	0.977265	0.989361	1.001515	1.000680

Table 3. *Values of* $J[R]/J_{\mathrm{ex}}$, *for Case 5 with* (BC_2).

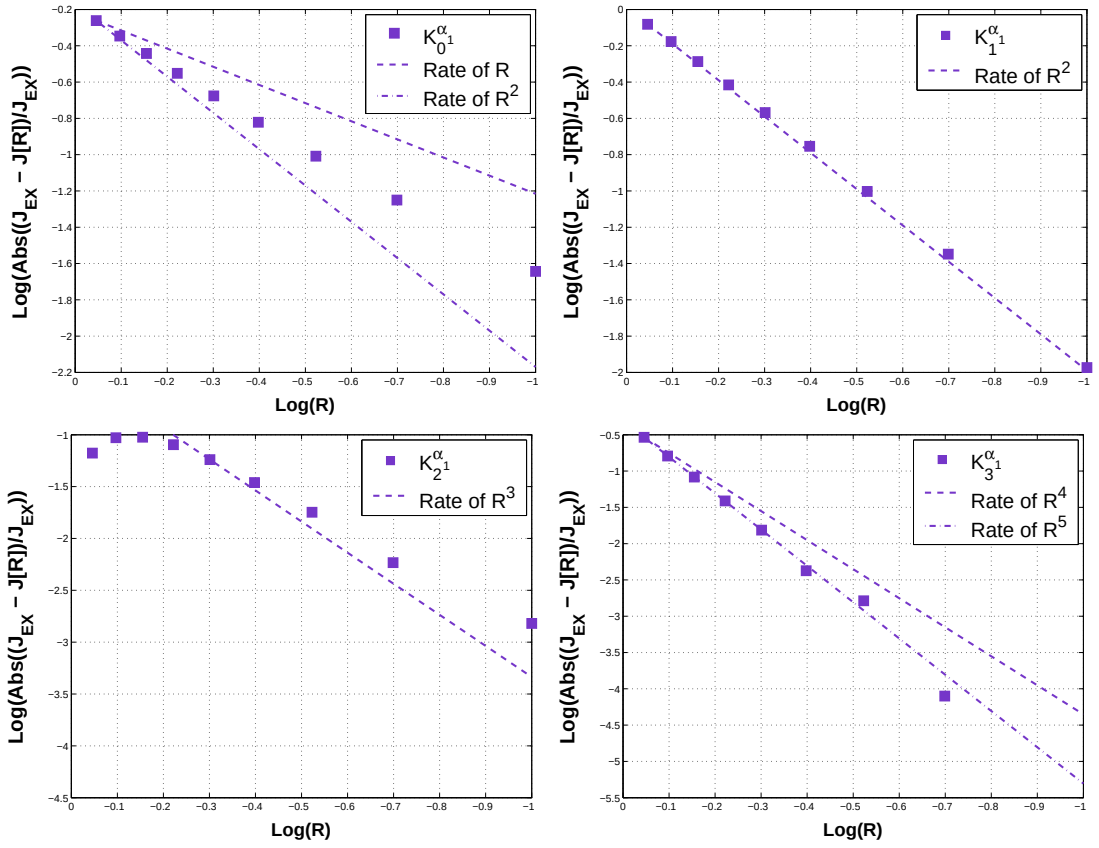

Figure 4. *Convergence rates of* $J[R]$ *for Case 5 with* (BC_2) *using* $K_m^{(\alpha_1)}$ *for* $m = 0,\, 1,\, 2,\, 3\,.$

We have performed numerical tests taking the boundary condition (BC_2), and computing $J[R]$ at different values of R with different choices of extraction polynomials B. We summarize the results in Table 3, and plot $\log(J_{\text{ex}} - J[R])$ vis. $\log(R)$ in Figure 4.

The results for $K_0^{(\alpha_1)}$ can be compared with those for Cases 1 - 4 in Table 2 and Figure 3. We see the lower convergence rate due to the presence of operator M_1, but this is dramatically improved by passing to the higher order quasidual functions $K_1^{(\alpha_1)}$ to $K_3^{(\alpha_1)}$.

We can see in Figure 4 that the convergence rate of $J[R]$ in Case 5 for $K_m^{(\alpha_1)}$ and B_m is at least of order R^{m+1} as we expected.

5. EFIF Extraction using Jacobi Polynomials

5.a Polynomial and non-polynomial EFIF

We are interested in extracting the EFIF $A^{(\alpha_i)}(x_3)$. Because its functional representation is unknown, its polynomial approximation is sought. We would like to construct an adaptive class of orthonormal polynomials with a given weight $w(x_3) = (1-x_3^2)^m$ so to represent $B_m(x_3)$. This suggests the use of Jacobi polynomials as a natural basis. In this way, if $A^{(\alpha_i)}(x_3)$ is a polynomial of degree N, it can be represented by a linear combination of Jacobi polynomials as:

$$A^{(\alpha_i)}(x_3) = \tilde{a}_0 J_m^{(0)} + \tilde{a}_1 J_m^{(1)}(x_3) + \cdots + \tilde{a}_N J_m^{(N)}(x_3) \tag{5.1}$$

where $J_m^{(k)}$ is the Jacobi polynomial of degree k and order m, i.e. associated with the weight $w(x_3) = (1-x_3^2)^m$, which is denoted in literature by $P_k^{(m,m)}$. There holds the following important orthogonality property [1, pp. 773-774] :

$$\int_{-1}^{1} (1-x_3^2)^m J_m^{(n)}(x_3) J_m^{(k)}(x_3)\, dx_3 = \delta_{nk} h_k \tag{5.2}$$

with some real coefficients h_k (depending on m). The hierarchical family of extraction polynomials, denoted by $BJ_m^{(k)}(x_3)$, has to be chosen so to satisfy $BJ_m^{(k)}(\pm 1) = \partial_3 BJ_m^{(k)}(\pm 1) = \cdots = \partial_3^{m-1} BJ_m^{(k)}(\pm 1) = 0$. To fulfil this, we set

$$BJ_m^{(k)}(x_3) = (1-x_3^2)^m \, \frac{J_m^{(k)}(x_3)}{h_k}\,, \tag{5.3}$$

so that, according to (5.2), we retrieve the coefficients $\tilde{a}_k$ in (5.1) as a simple scalar product:

$$\int_{-1}^{1} A^{(\alpha_i)}(x_3) BJ_m^{(k)}(x_3)\, dx_3 = \tilde{a}_k \qquad k = 0, 1, \ldots, N. \tag{5.4}$$

Thus, by virtue of Theorem 4.1, the $J[R]$ integral evaluated for the quasi-dual functions $K_m^{(\alpha_i)}[B_m]$ with the extraction polynomials $B_m = BJ_m^{(k)}$, $k = 0, 1, \ldots, N$ provide approximations of the coefficients $\tilde{a}_k$.

Of course, in general $A^{(\alpha_i)}(x_3)$ is an unknown function and we wish to find a projection of it into spaces of polynomials. It is expected that as we increase the polynomial space, the approximation is better.

The EFIF $A^{(\alpha_i)}(x_3)$ has an infinite Fourier expansion in the basis $J_m^{(k)}$ with a sequence of coefficents $\tilde{a}_k$:

$$A^{(\alpha_i)}(x_3) = \sum_{k\geq 0} \tilde{a}_k J_m^{(k)} \tag{5.5}$$

converging in the weighted space $L^2[w]$ with $w = (1-x_3^2)^m$. For each fixed n , the computation of the $n+1$ coefficients $\tilde{a}_0, \ldots, \tilde{a}_n$ provides the orthogonal projection of $A^{(\alpha_i)}(x_3)$ into the space of polynomials of degree up to n in the weighted space $L^2[w]$. To accomplish this we use the $n+1$ extraction polynomials $BJ_m^{(0)}(x_3), \ldots, BJ_m^{(n)}(x_3)$ defined in (5.3), so that there holds according to (5.2):

$$\int_{-1}^{1} A^{(\alpha_i)}(x_3) BJ_m^{(k)}(x_3)\, dx_3 = \tilde{a}_k \qquad k = 0, 1, \ldots, n. \tag{5.6}$$

If we want to increase the space in which $A^{(\alpha_i)}(x_3)$ is projected, all which is needed is the computation of (5.6) for $k = n+1$. This way: $A^{\text{new}}(x_3) = A^{\text{previous}}(x_3) + \tilde{a}_{n+1} J_{n+1}(x_3)$.

5.b Jacobi Extraction Polynomials of Order 2

Since they satisfy (4.8), and, a fortiori, (4.7) and (4.6), the Jacobi extraction polynomials $BJ_2^{(k)}$ can be combined with the dual singular functions $K_0^{(\alpha_i)}$, $K_1^{(\alpha_i)}$ and $K_2^{(\alpha_i)}$. There holds [1, pp. 773-774]:

$$J_2^{(k)}(x_3) = \frac{1}{k^2+7k+12} \sum_{l=0}^{k} \frac{(k+l+4)!}{2^l l!\,(k-l)!\,(2+l)!}\,(x_3-1)^l \tag{5.7}$$

and the constant h_k in (5.2) is equal to

$$h_k = \frac{2^5(k+1)(k+2)}{(2k+5)(k+3)(k+4)} \tag{5.8}$$

Inserting (5.8) and (5.7) in (5.3), we finally obtain:

$$BJ_2^{(k)}(x_3) = \frac{(2k+5)(k+3)(k+4)}{2^5(k+1)(k+2)} \frac{(1-x_3^2)^2}{k^2+7k+12} \sum_{l=0}^{k} \frac{(k+l+4)!}{2^l l!\,(k-l)!\,(2+l)!}\,(x_3-1)^l. \tag{5.9}$$

5.c Numerical results for (BC_4) using $K_2^{(\alpha_1)}$ with Jacobi Extraction Polynomials

For the benchmark problem with boundary conditions (BC_4) for which the exact EFIF is the polynomial (4.14) of degree 4 and using the extraction polynomials $BJ_2^{(0)}(x_3), \ldots, BJ_2^{(n)}(x_3)$, where $0 \leq n \leq 4$, we extract the EFIF for Case 2 at $R = 0.05$: We have performed the computation with 15 integration points and $p = 8$ in the finite element mesh, and present in Figure 5 the relative error in percentage between the extracted EFIF and the exact one. As may be seen for the family of degree 4 we indeed fully recover the exact EFIF.

Of course, if $n > 4$ we should fully recover the EFIF. As one increases the order of the hierarchical family, the results do not improve, but we obtain an oscillatory behavior of the solution due to numerical errors (the finite element solution is not exact), with a very small amplitude as demonstrated in Figure 6.

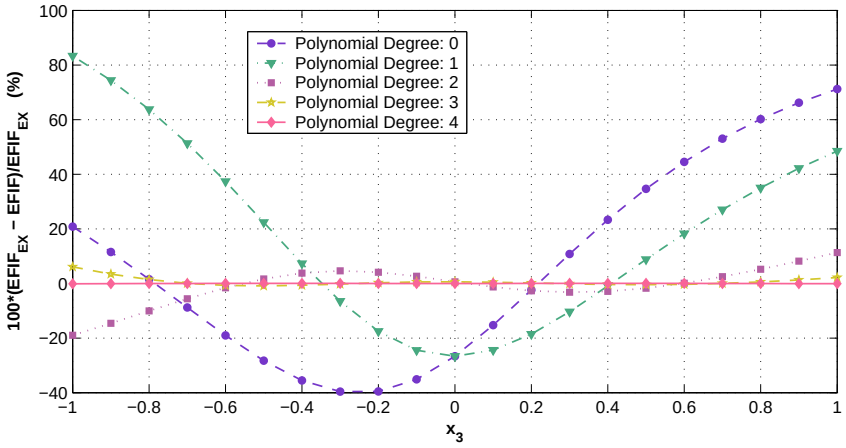

Figure 5. *Relative error (%) of the extracted EFIF at* $R = 0.05$ *using* $K_2^{(\alpha_1)}$ *and the hierarchical family* $BJ_2^{(k)}(x_3)$ *,* $k \leq n$ *, for* $n = 0,\ 1,\ 2,\ 3,\ 4$ *.*

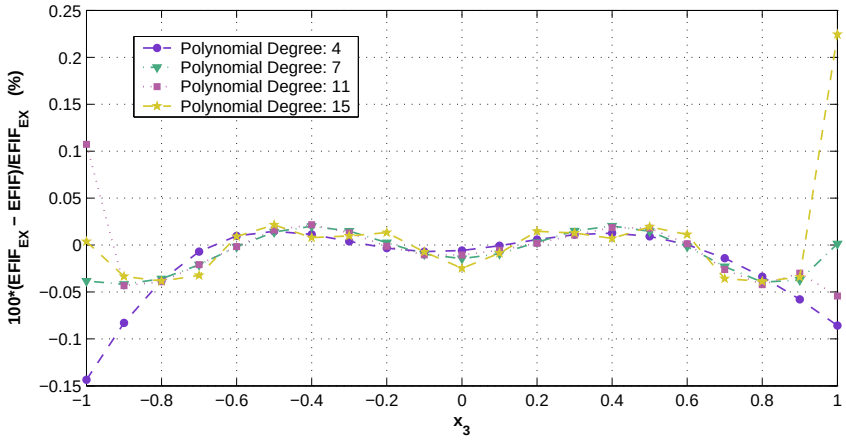

Figure 6. *Relative error (%) of the extracted EFIF at* $R = 0.05$ *using* $K_2^{(\alpha_1)}$ *and the hierarchical family* $BJ_2^{(k)}(x_3)$ *,* $k \leq n$ *, for* $n = 4,\ 7,\ 11,\ 11,\ 15$ *.*

To illustrate the convergence of the extracted values as a function of R, we present in Table 4 the monomial coefficients of the extracted polynomial at $R =$ 0.9, 0.5, 0.2, 0.05. Then we use Richardson's extrapolation, knowing that the error behaves as $\mathcal{O}(R^4)$, *cf* Remark 4.2, and the coefficients at $R =$ 0.9, 0.5 to extrapolate to $R = 0$. These extrapolation results are shown in the last column of Table 4. The relative error in the extrapolated EFIF using the data at $R = 0.9$, 0.5 is compared with that obtained at $R = 0.5$ and 0.05 in Figure 7.

	Exact	$R = 0.9$	$R = 0.5$	$R = 0.2$	$R = 0.05$	Extrapolated using $R = 0.9, 0.5$
a_0	5	5.920806968	5.089253508	5.005993235	5.000288235	5.001699446
a_1	4	4.004545148	4.002303539	4.002751475	3.998527960	4.002067521
a_2	9	9.047407703	9.008253090	9.001724824	8.989161317	9.004130510
a_3	3	2.985298783	2.995871625	3.001625541	3.005167695	2.996984837
a_4	1	0.904830390	0.983905020	1.007098452	1.025721321	0.992230769

Table 4. *Computed coefficients* a_i *for* (BC_4), *using* $K_2^{(\alpha_1)}$ *and* $BJ_2^{(k)}(x_3)$, $k \leq 4$.

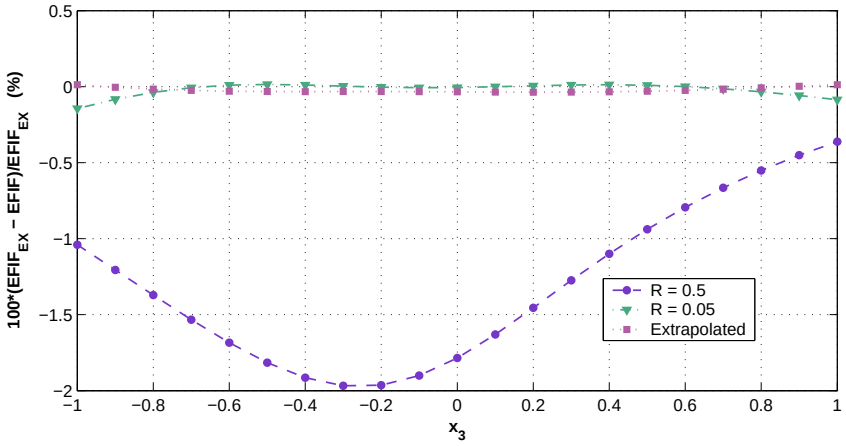

Figure 7. *Relative error (%) of the extracted EFIF at* $R = 0.5, 0.05$ *and extrapolating from data at* $R = 0.9, 0.5$. *EFIF computed using* $K_2^{(\alpha_1)}$ *and the hierarchical family* $BJ_2^{(k)}(x_3)$, $k \leq 4$.

By extracting the EFIF from the FE solution away from the singular edge (where usually the numerical data is polluted), we demonstrate that a very good approximation is obtained by Richardson's extrapolation, taking into consideration that the error behaves as $\mathcal{O}(R^4)$. Practically, the relative error in the extrapolated EFIF is as obtained very close to the singular edge ($R = 0.05$), and much better than the values obtained when extraction is performed at $R = 0.5$.

6. A Polynomial Representation of a Non-Polynomial EFIF

We have demonstrated so far that the quasi-dual extraction method performs very well if the exact EFIF is a polynomial. A natural question is - what if the EFIF is not a polynomial? In this case

we use the hierarchical algorithm for polynomial space enrichment described in §5.a. Herein we investigate the performance of such hierarchical space enrichment for the case where the exact EFIF is a general function, and furthermore, it contains high gradients at the ends of the edge. For example, consider Case 2, where the EFIF is a function of the form:

$$A^{(\alpha_1)}(x_3) = \frac{\sin x_3}{(d - x_3^2)} \tag{6.1}$$

where d is a given number. As d approaches 1, the EFIF approaches infinity at the vertices $x_3 = \pm 1$. We chose three values of $d = 2, 1.5, 1.05$.

Consider the following problem:

$$\left\{ \begin{array}{rcll} L(\tau) & = & \partial_3^2 A^{(\alpha_1)}(x_3)\Phi_0^{(\alpha_1)}(r,\theta) & \text{in} \quad \Omega \\ \tau & = & A^{(\alpha_1)}(x_3)\Phi_0^{(\alpha_1)}(r,\theta) & \text{on} \quad \partial\Omega, \end{array} \right. \tag{6.2}$$

for which the exact solution is simply $\tau_{\text{ex}} = A^{(\alpha_1)}(x_3)\Phi_0^{(\alpha_1)}(r,\theta)$.

Remark 6.1 *Theorem 4.1 does not apply stricto sensu to the solution of problem* (6.2)*. Nevertheless it can be proved that* $J[R](\tau, K_m^{(\alpha_i)}[B])$ *yields an approximation of the moment of* $A^{(\alpha_1)}$ *modulo a positive power of* R.

6.a Finite element approximation

A refined finite element model graded towards $x_3 = \pm 1$ was generated as shown in Figure 8. It has 25 elements in the x_3 direction and a total of 800 solid finite elements.

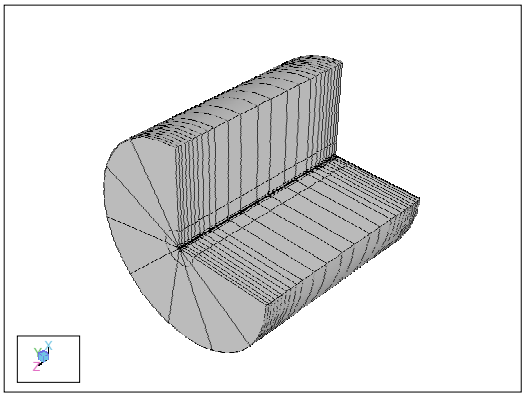

Figure 8. *The* p*-FEM model for non-polynomial EFIFs with large gradients at* $x_3 = \pm 1$.

To evaluate the accuracy of the extracted EFIFs, one has first to examine the numerical results, τ_{FE} and its derivatives, especially for solutions having large gradients. The graphs in Figure 9 present the relative error in τ_{FE} and $\partial_r \tau_{\text{FE}}$ in percentage, extracted from the finite element solution at $p = 8$ for $d = 2, 1.5, 1.05$. These graphs are along the line $R = 0.05$, $\theta = 135^\circ$ and $-1 \le x_3 \le 1$.

The FE results have a relative error of about 3% for $-0.8 \leq x_3 \leq 0.8$, and around 17% for $0.8 < |x_3| < 1$ for the case when $d = 1.05$. This in turn will perturb the extraction of the EFIF by that order of magnitude when using the quasi-dual extraction technique, as we show in the sequel. We will also observe that the EFIFs are computed with similar accuracy and the extraction technique does not magnify the numerical error but the opposite. For $d = 2$, 1.5, the relative error in the function and its derivatives is very small (less than 0.7%) in all the range. Therefore, the extraction of the EFIFs is expected to provide excellent results.

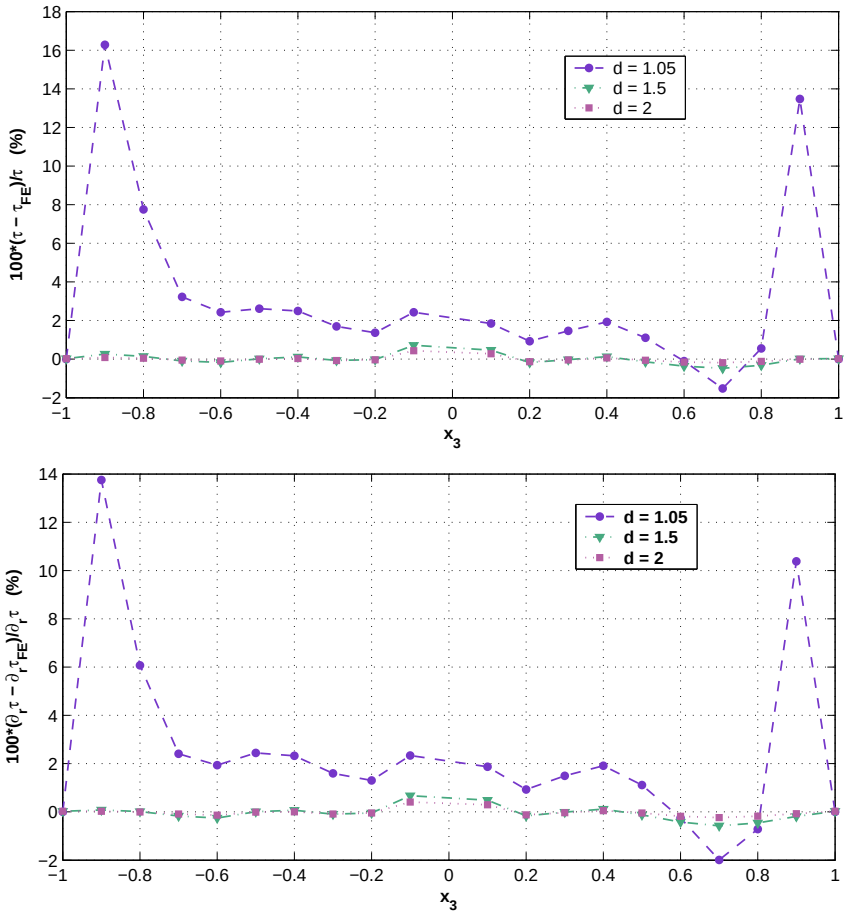

Figure 9. *Relative error in FE solution and its derivatives (%) at* $p = 8$ *for* $r = 0.05$, $\theta = 135°$, $x_3 \in [-1, 1]$ *for the three problems defined by* $d = 2$, 1.5 *and* 1.05.

6.b Extraction of EFIFs

Using $K_2^{(\alpha_1)}$ and the hierarchical family $BJ_2^{(k)}(x_3)$, we extract the EFIFs at $R = 0.05$ using the solution at $p = 8$ and 54 Gauss integration points (due to the strong gradients of the solutions we used a higher integration scheme). We also checked with 94 Gauss integration points that the integration error in evaluating $J[R]$ is negligible.

Figure 10 presents the exact EFIF and the extracted EFIF using $BJ_2^{(k)}(x_3)$, $k \leq n$, of increasing order n obtained at $R = 0.05$. Notice the different ordinate scales inside the three

graphs. One may easily observe the strong gradients of the EFIF at $x_3 = \pm 1$, especially for the case where $d = 1.05$.

Relative errors between the extracted EFIF and the exact value are presented in Figure 11 (here, again, the ordinate scales are different from each other). For all cases of d, the EFIF is progressively better approximated away from the large gradients ($\approx -0.85 \leq x_3 \leq -0.85$) as the order of the extraction polynomials (n) is increased.

At $n = 19$ the extracted EFIF has less than 3% relative error for the case when $d = 1.05$ and less than 0.5% relative error for the cases $d = 1.5$ and $d = 2$.

The large pointwise errors in the close neighborhood of the high gradients is expected.

6.c Localized Extraction of EFIFs

In the vicinity of a vertex (the intersection of the edge with another edge) it is a-priori known that the EFIF may have large gradients approaching either zero, infinity or a constant value as $\rho \to 0$ (ρ denotes the distance to the vertex). A detailed explanation on the decomposition of the solution in the vicinity of the edge as it approaches a vertex can be found in [10]. The asymptotic solution in the vicinity of the edge as presented in section 2 is therefore irrelevant on the entire edge I. It is expected therefore that better results can be obtained by approximating the EFIFs by polynomials on *an inner part* of the edge, for example at $a < x_3 < b$ where $-1 < a, b < 1$. This localized extraction strategy is a slight modification of the $J[R]$ integral, so that instead of integrating along a cylinder having its axis $I = [-1, 1]$, the integration is be performed along a cylinder with the axis $[a, b]$. The modification is easily implemented by a transformation of variables.

The localized extraction strategy has been investigated on Case 2 for problem (6.2) with the RHS as prescribed in by (6.1) and $d = 1.05$, for which the exact EFIF is given by:

$$A^{(\alpha_1)}(x_3) = \frac{\sin x_3}{(1.05 - x_3^2)} \,. \tag{6.3}$$

Using $K_2^{(\alpha_1)}$ and the hierarchical family $BJ_2^{(k)}(x_3)$ and the finite element model shown in Figure 8, we extract the EFIFs at R=0.05 using the solution at $p = 8$ and 54 Gauss integration points. The EFIFs are computed at three intervals on the edge: $-1 < x_3 < 1$, $-0.8 < x_3 < 0.8$ and $-0.6 < x_3 < 0.6$.

In Figure 12 we present the relative error in the extracted EFIF using $BJ_2^{(k)}(x_3)$ of order 4, 11 and 15. As expected, when the selected interval for EFIF extraction is reduced and confined in a region away from the high gradients, a much better approximation is obtained.

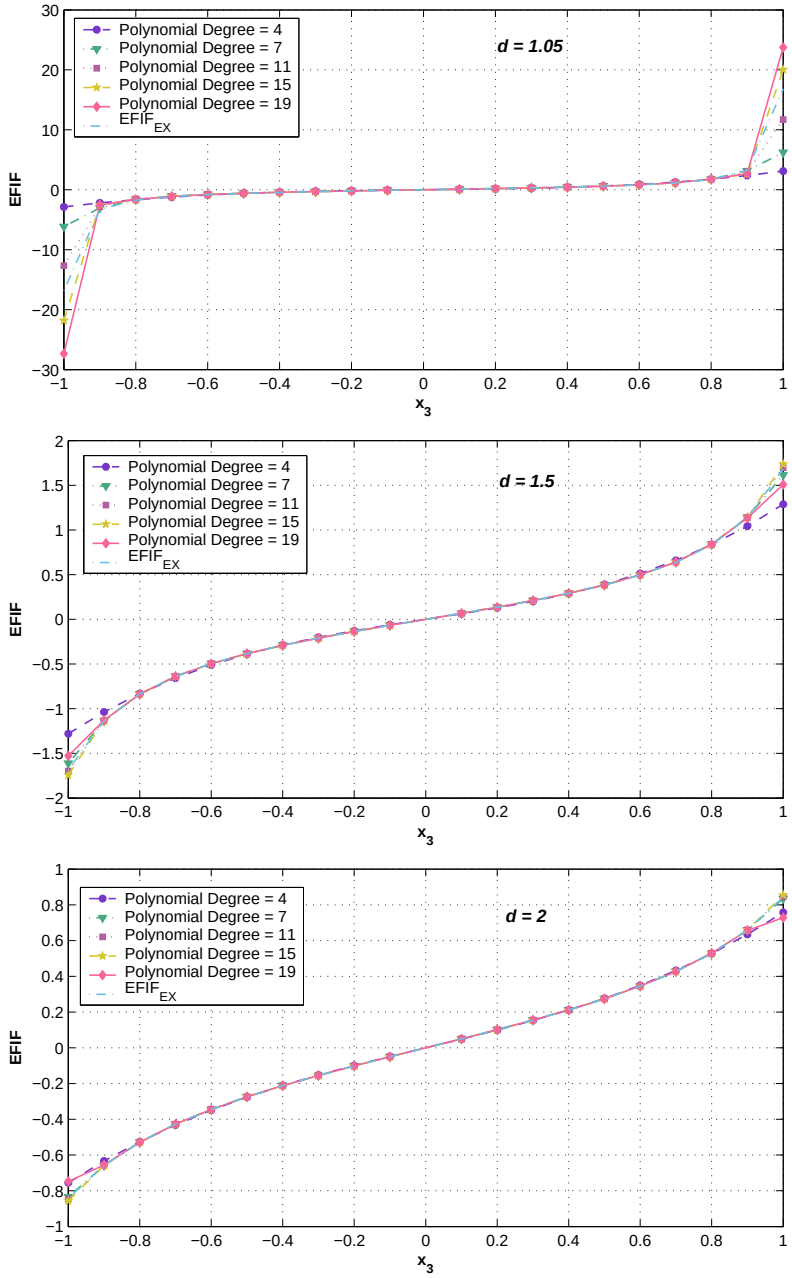

Figure 10. *Exact and extracted EFIF, using* $K_2^{(\alpha_1)}$ *and extraction polynomials of degree* $\leq n$ *for* $n = 4,\ 7,\ 11,\ 15,\ 19$ *.*

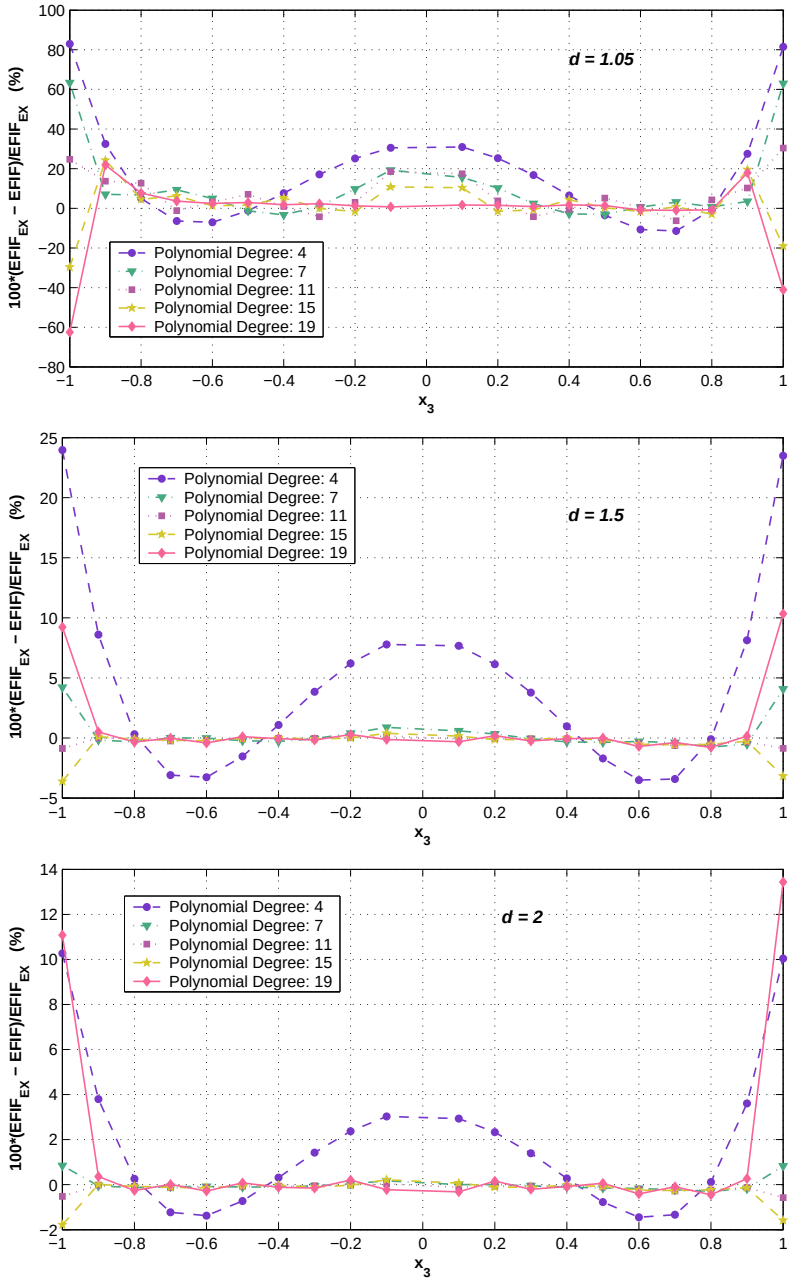

Figure 11. *Relative error (%) of extracted EFIF, using* $K_2^{(\alpha_1)}$ *and extraction polynomials of degree* $\leq n$ *for* $n = 4,\ 7,\ 11,\ 15,\ 19$.

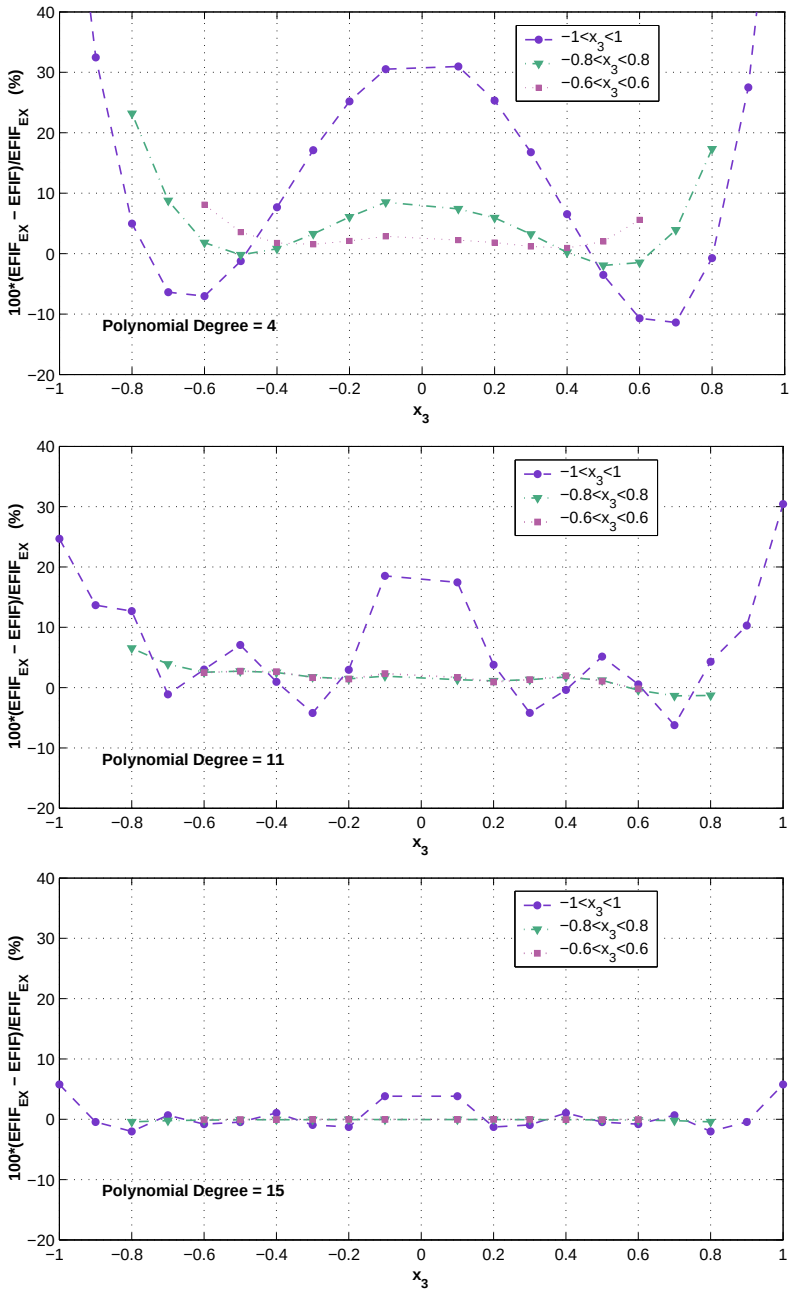

Figure 12. *Relative error (%) of extracted EFIF with the global and two partial extractions.*

7. A Domain with Vertices.

In order to examine the vertex influence on EFIF extraction we consider a more realistic domain constructed as an extension of the one presented in Figure 1 by adding two cylinders at ± 1 as shown in Figure 13. The added cylinders are $\Omega^{(1)} = D \times I^{(1)}$ and $\Omega^{(-1)} = D \times I^{(-1)}$ where $I^{(1)}$ is the interval $[1, 1.5]$, $I^{(-1)}$ is the interval $[-1.5, -1]$ and D is the disc of radius 1.

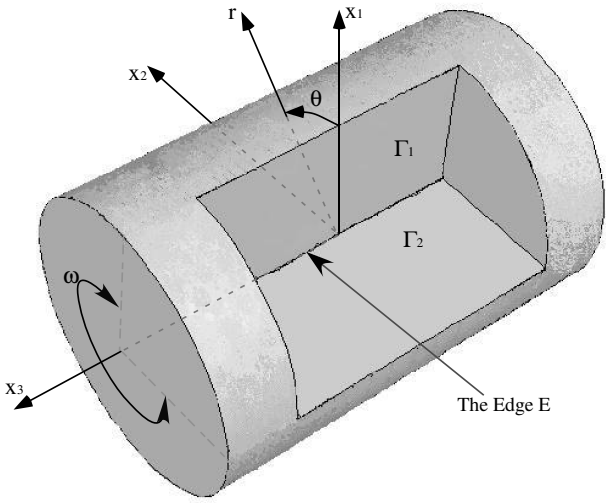

Figure 13. Schematic realistic domain with two Fichera corners.

The domain has been discretized by using a p-FEM mesh, with geometrical progression toward $r = 0$ with a factor of 0.15, having four layers of elements and towards $x_3 = \pm 1$, having 45 layers of elements. The discretization of the domain is presented in Figure 14.

We consider the Laplace equation. Homogeneous Neumann boundary conditions are prescribed over the domain's boundary, except for the following:

$$\frac{\partial \tau}{\partial r} = 1 \quad \text{on } \Gamma \tag{7.1}$$

$$\tau = 0 \quad \text{on } \Gamma_1 \cup \Gamma_2 \tag{7.2}$$

where:

$$\Gamma := \left\{ \boldsymbol{x} \in \mathbb{R}^3 \mid r = 1,\ \theta \in (0, \omega),\ x_3 \in (-1.5, 1.5) \right\}, \tag{7.3}$$

as shown in Figure 14. Under these boundary conditions, vertex singularities arise at $(r, \theta, x_3) = (0, 0, -1)$ and $(r, \theta, x_3) = (0, 0, 1)$ and the exact EFIF is unknown. It can be expected that the EFIF tends to infinity at the vertices.

Using the extraction polynomials $BJ_2^{(0)}, \ldots, BJ_2^{(k)}$, where $4 < k < 15$, we extract the EFIF for Case 1 at $R = 0.05$ on three intervals on the edge: $-1 < x_3 < 1$, $-0.9 < x_3 < 0.9$ and $-0.8 < x_3 < 0.8$. These are presented in Figure 15. It can be observed that the EFIFs extracted on $-1 < x_3 < 1$ are influenced by the vertex singularities at $x_3 = \pm 1$.

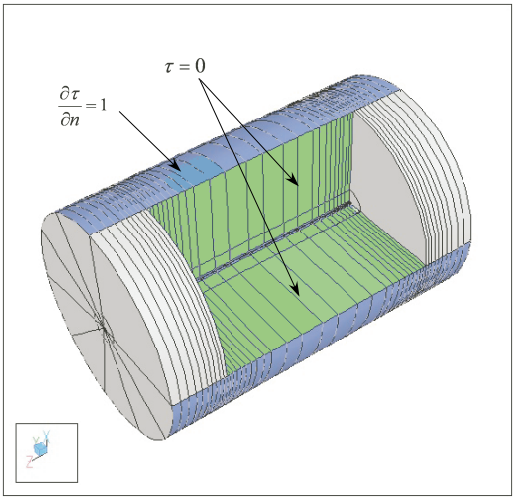

Figure 14. The boundary conditions (7.1)-(7.2) applied on the FE model.

8. Summary and Conclusions.

The EFIF extraction method presented herein is an extension of the 2-D contour integral method to 3-D domains, based on the mathematical framework which is presented in [8]. The method provides a functional (polynomial) representation of the EFIF along the edge. This accurate and efficient method is implemented as a post-solution operation in conjunction with the p-version finite element method.

A hierarchical family of extraction polynomials was constructed, based on Jacobi orthogonal polynomials. The quasi-dual function method, with the use of the "hierarchial family of polynomials" becomes adaptive in the sense that it uses a simple procedure to increase the degree of the extracted EFIF polynomial, thus enabling a reliable and efficient determination of EFIFs.

Analytical solutions have been constructed against which the extracted EFIFs were compared. As shown, the relative errors of the extracted EFIF were less than 1%, when the degree of the extracted EFIF polynomials is determined by an adaptive method, and Richardson extrapolation was used.

The extraction method uses finite element solutions and Gauss quadrature for the numerical integration. Both the finite element solution and the Gauss quadratures involve numerical errors. The errors were monitored and the results presented in Appendix C show that both the FEM errors and the numerical quadrature influence the accuracy of the extracted EFIF very little, when a high polynomial degree is used in the FEM approximation and the quadrate order is at least 10.

We also demonstrated that in the presence of vertices, and steep gradients in the EFIFs, one may use the localized extraction method when applying the $J[R]$ integral, thus improving the accuracy over the sub-intervals of the edge where the EFIF are of interest.

The results presented herein indicate that the method proposed for EFIF extraction is accurate and efficient. It is being extended to elastic problems in polyhedral domains where the edge stress intensity functions (ESIFs) are described by a 1×3 vector associated with eigen-functions and their shadows. Although technically more cumbersome, same steps as presented herein carry over to the elastic Navier-Lamé system of equations. The Navier-Lamé operator (represented by a 3×3 matrix containing derivatives) is being split into three matrices, based on which the eigen-

functions their duals and shadows are determined analytically for isotropic materials. These may contain complex eigen-pairs appearing in conjugates. Using the eigen-pairs, their duals and the associated shadows, in conjunction with the developed polynomial extraction functions presented herein, the $J[R]$ integral can be applied so to obtain ESIFs. Extension of this work to traction free boundary conditions associated with elastic problems of engineering importance (according to the mentioned milestones) will be reported in a subsequent paper. These ESIFs are of particular interest in three dimensional elastic domains along the front of a crack or a V-notch, because they are used in failure laws (see e.g. [11, 18]).

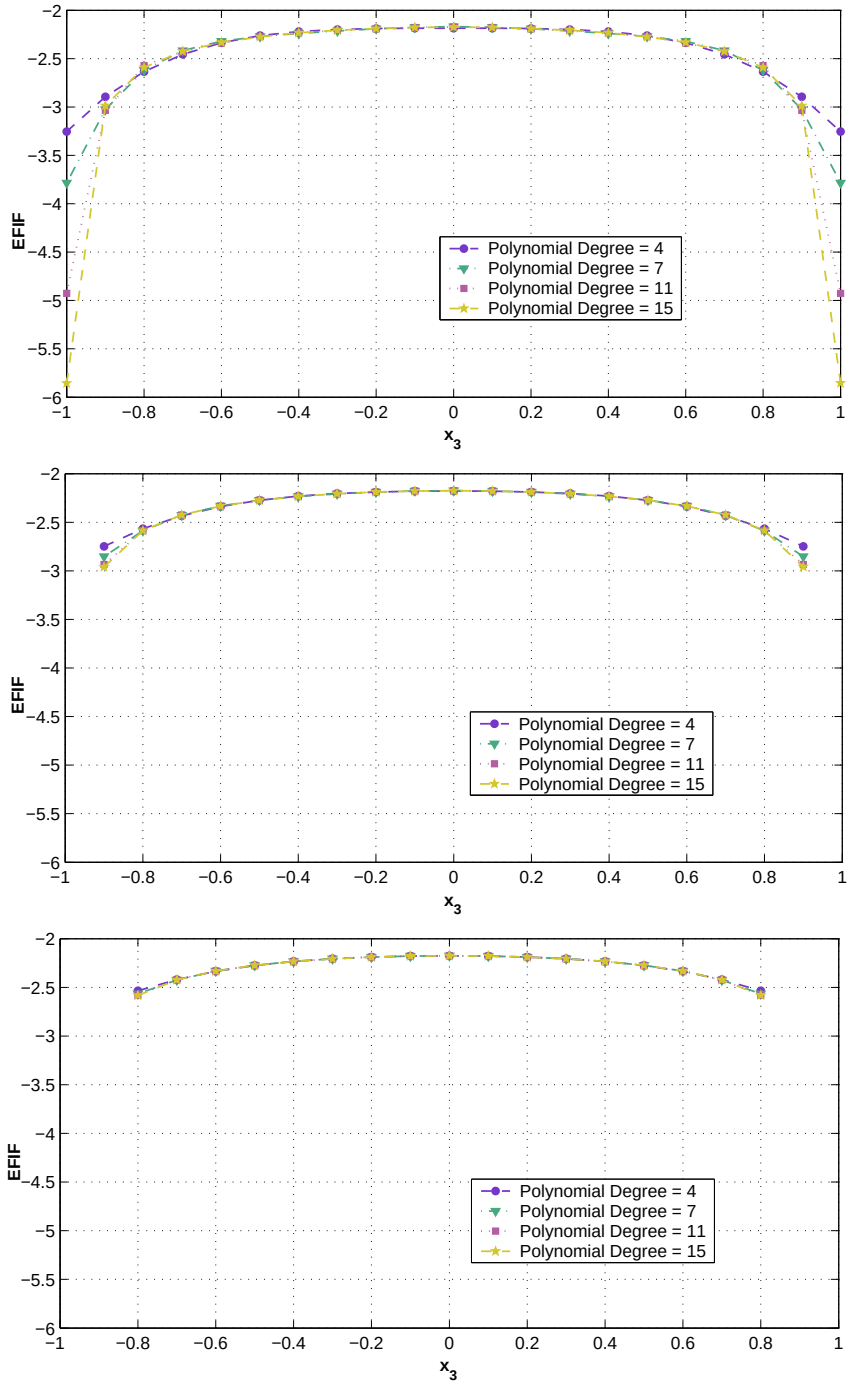

Figure 15. *Top: EFIF extracted on* $-1 < x_3 < 1$. *Middle: EFIF extracted on* $-0.9 < x_3 < 0.9$. *Bottom: EFIF extracted on* $-0.8 < x_3 < 0.8$. *All using the hierarchical extraction polynomials of degree* $k = 4,\ 7,\ 11,\ 15$, *with* $K_2^{(\alpha_1)}$ *at* $R = 0.05$.

Appendix A
The Primal and Dual Eigen-functions and Their Shadows for Cases 1-4.

For the Cases 1 - 4 the operator L can be split as in (3.5) with:

$$M_0 = k_{11}\partial_1\partial_1 + 2k_{12}\partial_1\partial_2 + k_{22}\partial_2\partial_2, \quad M_1 = 0, \quad M_2 = 1 \tag{A1}$$

Aa Computing the primal and dual eigen-functions Φ_0 and Ψ_0 :

Φ_0 and Ψ_0 are the solutions of the first equation in (3.5), where the operator is M_0 on the plane domain G. A change of variables is performed:

$$\xi(x_1, x_2) = \sqrt{\frac{k_{22}}{k_{11}k_{22} - k_{12}^2}}x_1 - \sqrt{\frac{k_{12}^2}{k_{22}(k_{11}k_{22} - k_{12}^2)}}x_2 \tag{A2}$$

$$\eta(x_1, x_2) = \sqrt{\frac{1}{k_{22}}}x_2 \tag{A3}$$

so that M_0 in the new variables is transformed into the Laplace operator:

$$\frac{\partial^2}{\partial\xi^2} + \frac{\partial^2}{\partial\eta^2}, \tag{A4}$$

over a plane domain G'. The straight lines defined by $\theta = 0$ and $\theta = \omega$ in the original domain G are transformed into the two lines defined by $\gamma = 0$ and $\gamma = \omega^*$ in the transformed domain G' where:

$$\omega^* = \arctan\left(\frac{\sqrt{k_{11}k_{22} - k_{12}^2}\sin\omega}{k_{22}\cos\omega - k_{12}\sin\omega}\right) \tag{A5}$$

as illustrated in Figure 16. Both Φ_0 and Ψ_0 have to satisfy homogeneous Dirichlet boundary

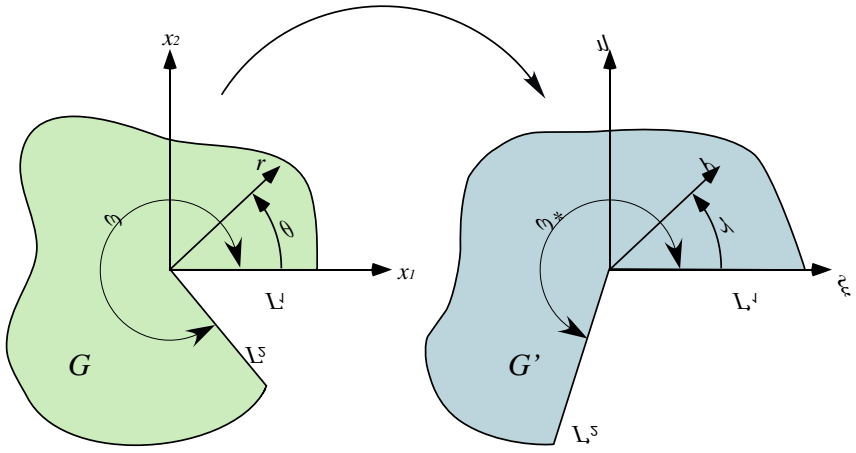

Figure 16. The plane domain G before and after change of variables.

conditions on $\theta = 0, \omega$ in the original domain, which become in the transformed domain:

$$\Phi_0(\rho, 0) = \Phi_0(\rho, \omega^*) = \Psi_0(\rho, 0) = \Psi_0(\rho, \omega^*) = 0. \tag{A6}$$

The solutions to the Laplace equation (by separation of variables) are:

$$\begin{cases} \Phi_0(\rho,\gamma) = \rho^{\alpha}\left(A\cos(\alpha\gamma) + B\sin(\alpha\gamma)\right) \\ \Psi_0(\rho,\gamma) = c_0\rho^{-\alpha}\left(A\cos(\alpha\gamma) - B\sin(\alpha\gamma)\right) \end{cases} \tag{A7}$$

where Φ is associated with the positive eigen-values and Ψ is associated the negative eigen-values. The value of the constant c_0 is chosen so to satisfy an orthonormal condition as will be discussed next. Equation (A6) results in (here we provide the equations for Φ_0, although same ones are obtained for Ψ_0):

$$\begin{pmatrix} 1 & 0 \\ \cos(\alpha\omega^*) & \sin(\alpha\omega^*) \end{pmatrix} \begin{pmatrix} A \\ B \end{pmatrix} = \begin{pmatrix} 0 \\ 0 \end{pmatrix} \tag{A8}$$

For a non-trivial solution, α has to satisfy:

$$\alpha_i = \pm\frac{i\pi}{\omega^*}, \qquad i = 1,2,\ldots \tag{A9}$$

There are an infinite number of distinct α_i's, for which there is an associated $\Phi_0^{(\alpha_i)}$ and $\Psi_0^{(\alpha_i)}$, and distinct B_i where:

$$A_i = 0$$

The generic constant is omitted, as it is added to the EFIF in the asymptotic expansion. To obtain the solution in the original domain G, a reverse transformation of variables is performed and the functions $\Phi_0^{(\alpha_i)}$ and $\Psi_0^{(\alpha_i)}$ are obtained in the coordinates r,θ:

$$\Phi_0^{(\alpha_i)}(r,\theta) = r^{\alpha_i}\varphi_0^{(\alpha_i)}(\theta), \qquad \Psi_0^{(\alpha_i)}(r,\theta) = c_0^{(\alpha_i)}r^{-\alpha_i}\psi_0^{(\alpha_i)}(\theta)$$

where

$$\varphi_0^{(\alpha_i)}(\theta) = \left(\frac{k_{22}\cos^2\theta - k_{12}\sin(2\theta) + k_{11}\sin^2\theta}{k_{11}k_{22}-k_{12}^2}\right)^{\frac{\alpha_i}{2}} \sin\left(\alpha_i \arctan\left(\frac{\sqrt{k_{11}k_{22}-k_{12}^2}\sin\theta}{k_{22}\cos\theta - k_{12}\sin\theta}\right)\right)$$

and

$$\psi_0^{(\alpha_i)}(\theta) = \left(\frac{k_{22}\cos^2\theta - k_{12}\sin(2\theta) + k_{11}\sin^2\theta}{k_{11}k_{22}-k_{12}^2}\right)^{-\frac{\alpha_i}{2}} \sin\left(\alpha_i \arctan\left(\frac{\sqrt{k_{11}k_{22}-k_{12}^2}\sin\theta}{k_{22}\cos\theta - k_{12}\sin\theta}\right)\right)$$

One may notice that for the Laplace operator, $k_{ij} = \delta_{ij}$, then $\omega^* = \omega$ and the eigen-functions and their duals are the well known expressions:

$$\begin{cases} \Phi_0^{(\alpha_i)}(r,\theta) = r^{\alpha_i}\varphi_0^{(\alpha_i)}(\theta) = r^{\alpha_i}\sin(\alpha_i\theta) \\ \Psi_0^{(\alpha_i)}(r,\theta) = c_0^{(\alpha_i)}r^{-\alpha_i}\psi_0^{(\alpha_i)}(\theta) = c_0^{(\alpha_i)}r^{-\alpha_i}\sin(\alpha_i\theta) \end{cases} \quad , \quad \alpha_i = \frac{i\pi}{\omega}.$$

Ab The value of the constant $c_0^{(\alpha_i)}$:

The value of the constant $c_0^{(\alpha_i)}$ is chosen such that the primal and the dual eigen-function, $\Phi_0^{(\alpha_i)}$ and $\Psi_0^{(\alpha_i)}$, satisfy the orthonormal condition:

$$\int_0^{\omega} \left[T(R)\Phi_0^{(\alpha_i)} \cdot \Psi_0^{(\alpha_i)} - \Phi_0^{(\alpha_i)} \cdot T(R)\Psi_0^{(\alpha_i)}\right] R\, d\theta = 1 \tag{A10}$$

where $T(R)$ is the radial Neumann trace operator related to the operator M_0 :

$$T(R) = \big(k_{11}\cos^2\theta + k_{12}\sin 2\theta + k_{22}\sin^2\theta\big)\tfrac{\partial}{\partial r} + \big(k_{12}\cos 2\theta - \tfrac{1}{2}(k_{11}-k_{22})\sin 2\theta\big)\tfrac{1}{r}\tfrac{\partial}{\partial\theta}\,.$$

Further details about (A10) are given in [8]. The value of the constant $c_0^{(\alpha_i)}$, is extracted from equation (A10):

$$c_0^{(\alpha_i)} = \left(\int_0^{\omega}\Big[T(R)\big(r^{\alpha_i}\phi_0^{(\alpha_i)}\big)\cdot\big(r^{-\alpha_i}\psi_0^{(\alpha_i)}\big) - \big(r^{\alpha_i}\phi_0^{(\alpha_i)}\big)\cdot T(R)\big(r^{-\alpha_i}\psi_0^{(\alpha_i)}\big)\Big]\,R\,d\theta\right)^{-1}.$$

One may notice that for the Laplace operator $k_{ij}=\delta_{ij}$ the Neumann trace operator simplifies to $T=\frac{\partial}{\partial r}$ and $c_0^{(\alpha_i)} = \frac{1}{\alpha_i\omega}$, which is the known coefficient of the dual eigen-function for a two dimensional domain. The explicit value of the constant $c_0^{(\alpha_1)}$ for Cases 1-4 is computed and presented in Table 5.

Ac The odd shadow functions and the odd dual shadow functions:

Once the primal eigen-function, $\Phi_0^{(\alpha_i)}$, is obtained, the first shadow function $\Phi_1^{(\alpha_i)}$ may be calculated by the second equation in (3.5). Because $M_1\equiv 0$, the differential equation is homogenous with homogeneous Dirichlet boundary conditions and therefore the first shadow function vanishes:

$$\Phi_1^{(\alpha_i)} = 0 \tag{A11}$$

The sequence of odd shadow functions, $\Phi_k^{(\alpha_i)}$ (where $k=3,5,7,\dots$), are calculated as the solution of the third equation in (3.5). For $\Phi_3^{(\alpha_i)}$ we obtain:

$$M_0\Phi_3^{(\alpha_i)} = -M_2\Phi_1^{(\alpha_i)} = 0 \tag{A12}$$

Once again the differential equation becomes homogeneous with homogeneous Dirichlet boundary conditions so that $\Phi_3^{(\alpha_i)}=0$. Same arguments hold for all odd shadow functions associated with an operator L having $k_{13}=k_{23}=0$, thus:

$$\Phi_k^{(\alpha_i)} = 0 \qquad k=3,5,7,\dots \tag{A13}$$

Computation of the dual shadow functions, $\Psi_k^{(\alpha_i)}$, is along the same lines thus for any L with $k_{13}=k_{23}=0$:

$$\Psi_k^{(\alpha_i)} = 0 \qquad k=3,5,7,\dots \tag{A14}$$

Ad The shadow function $\Phi_2^{(\alpha_i)}$ and its dual $\Psi_2^{(\alpha_i)}$:

The shadow function $\Phi_2^{(\alpha_i)}$ and its dual $\Psi_2^{(\alpha_i)}$ are the solution of the third equation in (3.5) with $j=0$. It is a non-homogeneous differential equation over a two dimensional domain with homogeneous Dirichlet boundary conditions. Its explicit form in coordinates ρ,γ is:

$$\left(\frac{\partial^2}{\partial\rho^2} + \frac{1}{\rho}\frac{\partial}{\partial\rho} + \frac{1}{\rho^2}\frac{\partial^2}{\partial\gamma^2}\right)\Phi_2^{(\alpha_i)} = -\rho^{\alpha_i}\sin(\alpha_i\gamma) \tag{A15}$$

The homogeneous solution is:

$$\Phi_2^{(\alpha_i)H} = \rho^f\left[A^H\cos(f\gamma) + B^H\sin(f\gamma)\right] \tag{A16}$$

and the particular solution is:

$$\Phi_2^{(\alpha_i)P} = \frac{-1}{4(\alpha_i+1)}\rho^{\alpha_i+2}\sin(\alpha_i\gamma) \tag{A17}$$

The particular solution identically satisfies the homogeneous Dirichlet boundary conditions so that the homogeneous solution must satisfy these:

$$\begin{cases} \Phi_2^{(\alpha_i)}(\rho,0) = \Phi_2^{(\alpha_i)H}(\rho,0) + \Phi_2^{(\alpha_i)P}(\rho,0) = \Phi_2^{(\alpha_i)H}(\rho,0) = 0 \\ \Phi_2^{(\alpha_i)}(\rho,\omega^*) = \Phi_2^{(\alpha_i)H}(\rho,\omega^*) + \Phi_2^{(\alpha_i)P}(\rho,\omega^*) = \Phi_2^{(\alpha_i)H}(\rho,\omega^*) = 0 \end{cases} \tag{A18}$$

The coefficients A^H, B^H vanish so that Φ_2 is the particular solution alone. We may conclude that $\Phi_2^{(\alpha_i)}$ is given by:

$$\Phi_2^{(\alpha_i)}(r,\theta) = r^{\alpha_i+2}\varphi_2^{(\alpha_i)}(\theta) \tag{A19}$$

where:

$$\varphi_2^{(\alpha_i)}(\theta) = -\frac{1}{4(\alpha_i+1)}\left(\frac{k_{22}\cos^2\theta - k_{12}\sin(2\theta) + k_{11}\sin^2\theta}{k_{11}k_{22}-k_{12}^2}\right)^{\frac{\alpha_i+2}{2}} \sin\left\{\alpha_i \arctan\left(\frac{\sqrt{k_{11}k_{22}-k_{12}^2}\sin\theta}{k_{22}\cos\theta - k_{12}\sin\theta}\right)\right\}.$$

Computing $\Psi_2^{(\alpha_i)}$ follows same arguments and we obtain:

$$\Psi_2^{(\alpha_i)}(r,\theta) = c_0^{(\alpha_i)} r^{\alpha_i+2}\psi_2^{(\alpha_i)}(\theta) \tag{A20}$$

where:

$$\psi_2^{(\alpha_i)}(\theta) = \frac{1}{4(\alpha_i-1)}\left(\frac{k_{22}\cos^2\theta - k_{12}\sin(2\theta) + k_{11}\sin^2\theta}{k_{11}k_{22}-k_{12}^2}\right)^{\frac{-\alpha_i+2}{2}} \sin\left\{\alpha_i \arctan\left(\frac{\sqrt{k_{11}k_{22}-k_{12}^2}\sin\theta}{k_{22}\cos\theta - k_{12}\sin\theta}\right)\right\}.$$

Ae The shadow function $\Phi_4^{(\alpha_i)}$:

The shadow function $\Phi_4^{(\alpha_i)}$ is generated by the third differential equation in (3.5) with $j = 2$. The method of extracting $\Phi_4^{(\alpha_i)}$ is very similar to the method of $\Phi_2^{(\alpha_i)}$ extraction. The explicit form of the differential equation in ρ, γ coordinates is:

$$\left(\frac{\partial^2}{\partial\rho^2} + \frac{1}{\rho}\frac{\partial}{\partial\rho} + \frac{1}{\rho^2}\frac{\partial^2}{\partial\gamma^2}\right)\Phi_4^{(\alpha_i)} = \frac{-1}{4(\alpha_i+1)}\rho^{\alpha_i+2}\sin(\alpha_i\gamma). \tag{A21}$$

The solution of $\Phi_4^{(\alpha_i)}$ is based on the particular solution alone since the homogeneous solution vanishes under the homogeneous Dirichlet boundary conditions. The shadow function $\Phi_4^{(\alpha_i)}$ in r, θ polar coordinates is:

$$\Phi_4^{(\alpha_i)}(r,\theta) = r^{\alpha_i+4}\varphi_4^{(\alpha_i)}(\theta) \tag{A22}$$

where:

$$\varphi_4^{(\alpha_i)}(\theta) = \frac{1}{32(\alpha_i+1)(\alpha_i+2)}\left(\frac{k_{22}\cos^2\theta - k_{12}\sin(2\theta) + k_{11}\sin^2\theta}{k_{11}k_{22}-k_{12}^2}\right)^{\frac{\alpha_i+4}{2}} \sin\left\{\alpha_i \arctan\left(\frac{\sqrt{k_{11}k_{22}-k_{12}^2}\sin\theta}{k_{22}\cos\theta - k_{12}\sin\theta}\right)\right\}.$$

Case #	ω^*	α_1	$c_0^{(\alpha_1)}$
Case 1	1.5π	2/3	0.31831
Case 2	1.1476π	0.87139	0.26903
Case 3	2.0π	0.5	0.31831
Case 4	2.0π	0.5	0.23533

Table 5. *Main coefficients of the considered cases*

Af The specific cases (1-4) eigen-functions:

The eigen-functions and the dual eigen-functions are defined by the eigen-value, α_i, the representative coefficient of the domain, ω^* (equation (A5), and the representative coefficient of the dual solution, $c_0^{(\alpha_i)}$. The coefficients of the selected cases, related with the first eigen-value are presented in Table 5.

We provide in Figures 17-20 the graphical representation of the primal and dual eigen-functions $\varphi_0^{(\alpha_1)}, \varphi_2^{(\alpha_1)}, \varphi_4^{(\alpha_1)}, \psi_0^{(\alpha_1)}, \psi_2^{(\alpha_1)}$ for Cases 1-4.

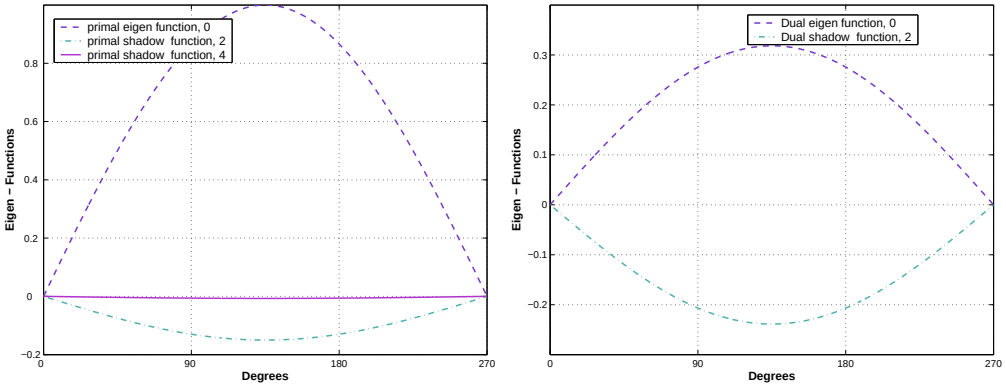

Figure 17. *The eigen-functions and dual eigen-functions associated with* α_1 *, for Case 1.*

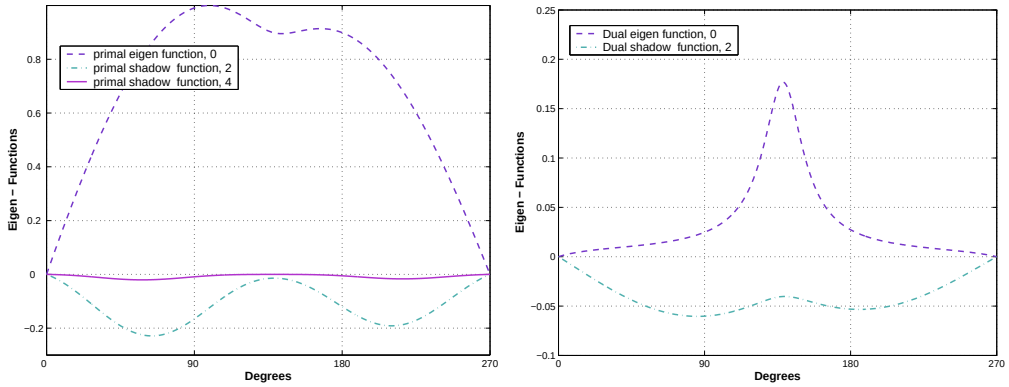

Figure 18. *The eigen-functions and dual eigen-functions associated with* α_1 *, for Case 2.*

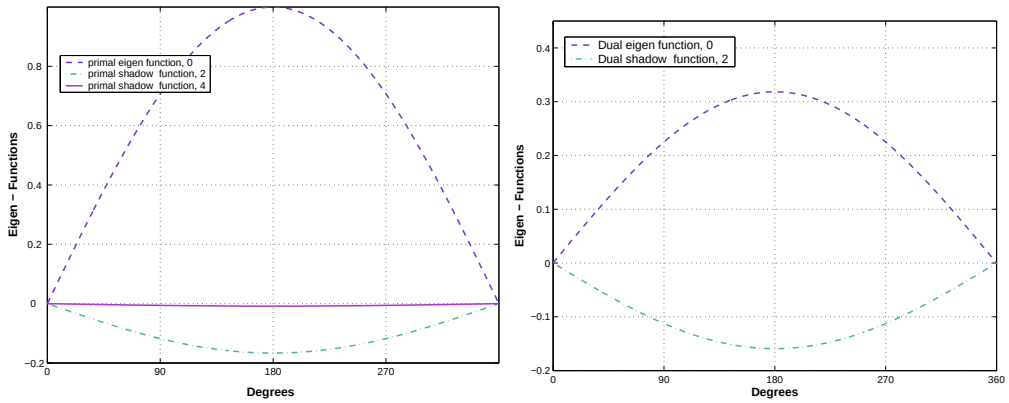

Figure 19. *The eigen-functions and dual eigen-functions associated with* α_1 *, for Case 3.*

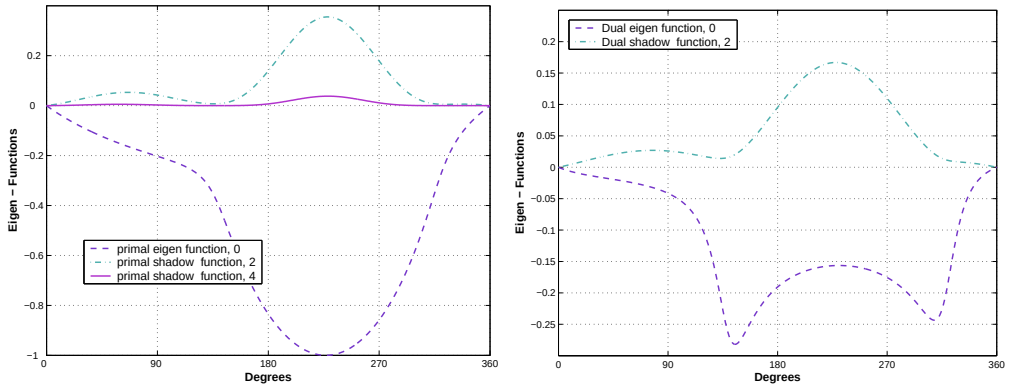

Figure 20. *The eigen-functions and dual eigen-functions associated with* α_1 *, for Case 4.*

Appendix B
The Primal and Dual Eigen-functions and Their Shadows for Cases 5.

The operator L for Case 5, is:

$$L = \partial_1\partial_1 + \partial_2\partial_2 - \partial_1\partial_3 + \partial_3\partial_3$$

with:

$$M_0 = \partial_1\partial_1 + \partial_2\partial_2 \quad M_1 = -\partial_1 \quad M_2 = 1$$

For this case $\Phi_0^{(\alpha_i)}$ and $\Psi_0^{(\alpha_i)}$ according to the first equation of system (3.5) are:

$$\Phi_0^{(\alpha_i)}(r,\theta) = r^{\alpha_i}\sin(\alpha_i\theta) \tag{B1}$$

$$\Psi_0^{(\alpha_i)}(r,\theta) = c_0^{(\alpha_i)} r^{-\alpha_i}\sin(\alpha_i\theta) \tag{B2}$$

with $\alpha_i = \frac{i\pi}{\omega}$, $i = 1, 2, \ldots$. The Neumann trace operator for Case 5 is simply $T = \frac{\partial}{\partial r}$ and therefore the coefficient of the dual solution is $c_0^{(\alpha_i)} = \frac{1}{\alpha_i\omega}$.

The shadow function $\Phi_1^{(\alpha_i)}$ is computed by the second differential equation of the system (3.5) and the shadow functions $\Phi_2^{(\alpha_i)}$ and $\Phi_3^{(\alpha_i)}$ are computed by the third differential equation of (3.5) with $j = 0$ and $j = 1$ respectively.

$$\Phi_1^{(\alpha_i)}(r,\theta) = \tfrac{1}{4}\, r^{\alpha_i+1}\Big(\sin(\alpha_i-1)\theta + \sin(\alpha_i+1)\theta\Big)$$

$$\Phi_2^{(\alpha_i)}(r,\theta) = \tfrac{1}{32}\, r^{\alpha_i+2}\Big(\sin(\alpha_i-2)\theta + \sin(\alpha_i+2)\theta + \tfrac{2(\alpha_i-2)}{\alpha_i+1}\sin\alpha_i\theta\Big)$$

$$\Phi_3^{(\alpha_i)}(r,\theta) = \tfrac{1}{384}\, r^{\alpha_i+3}\Big(\sin(\alpha_i-3)\theta + \sin(\alpha_i+3)\theta + \tfrac{3(\alpha_i-5)}{\alpha_i+1}\Big\{\sin(\alpha_i+1)\theta + \sin(\alpha_i-1)\theta\Big\}\Big).$$

The dual shadow function $\Psi_1^{(\alpha_i)}$ is computed by the second equation of the system (3.5) with Dirichlet boundary conditions. The shadow functions $\Psi_2^{(\alpha_i)}$ and $\Psi_3^{(\alpha_i)}$ are computed by the third differential equation of the system (3.5) with $j = 0$ and $j = 1$ respectively.

$$\Psi_1^{(\alpha_i)}(r,\theta) = \tfrac{1}{4}\, c_0^{(\alpha_i)} r^{-\alpha_i+1}\Big(\sin(\alpha_i-1)\theta + \sin(\alpha_i+1)\theta\Big)$$

$$\Psi_2^{(\alpha_i)}(r,\theta) = \tfrac{1}{32}\, c_0^{(\alpha_i)} r^{-\alpha_i+2}\Big(\sin(\alpha_i-2)\theta + \sin(\alpha_i+2)\theta + \tfrac{2(\alpha_i+2)}{\alpha_i-1}\sin\alpha_i\theta\Big)$$

$$\Psi_3^{(\alpha_i)}(r,\theta) = \tfrac{1}{384}\, c_0^{(\alpha_i)} r^{-\alpha_i+3}\Big(\sin(\alpha_i-3)\theta + \sin(\alpha_i+3)\theta + \tfrac{3(\alpha_i+5)}{\alpha_i-1}\Big\{\sin(\alpha_i+1)\theta + \sin(\alpha_i-1)\theta\Big\}\Big).$$

Figures 21 present the eigen-functions, their shadows and their duals associated with the first eigen-value for Case 5.

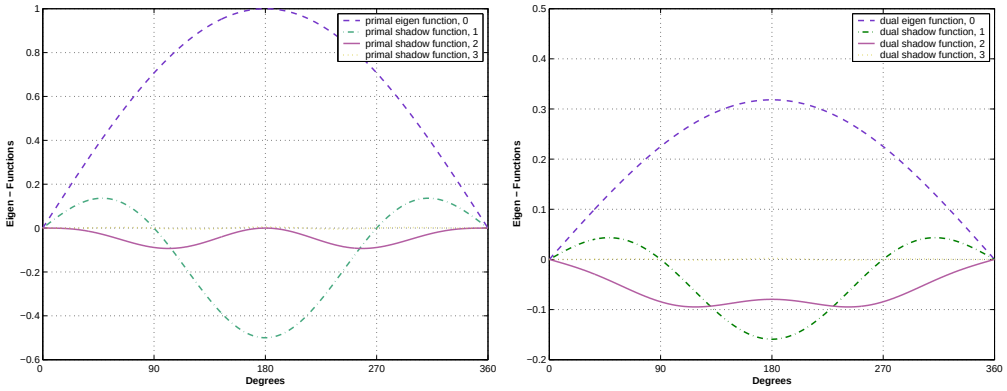

Figure 21. The eigen-functions and dual eigen-functions associated with the first eigen-value, α_1 , for Case 5.

Appendix C
Numerical Errors due to Numerical Integration and Finite Element Approximation.

The integral $J[R]$ is computed by a Gaussian quadrature, and using the approximated finite element solution instead of the exact solution. These incorporate numerical inaccuracies in our computations which should be controlled and bounded. We use Case 5 in this Section to quantify the level of numerical errors, and demonstrate that these are negligible.

Ca Errors due to Finite Element Approximation

By using a finite element solution as an approximation of the exact solution, a numerical error is included in our computations. In order to evaluate the influence of the error, we compute $J[R]$ at different polynomial degrees of the test and trial functions of the finite elements. The results summarized in Table 6 are the values of $J[R]/J_{\rm ex}$ for Case 5 with (BC_2) (*cf* §4.b), using the quasi-dual functions $K_0^{(\alpha_1)}$ to $K_3^{(\alpha_1)}$ with "proper" $B(x_3)$. The values of $J[R]/J_{\rm ex}$ are not influenced by the polynomial degree of the finite element approximation when using high degree of polynomial ($p = 5$ or higher).

$B(x_3)$	1	(x_3-1)	$(x_3-1)^2$	$(x_3-1)^3$
$J_{\rm ex}$	$8/3$	$-8/5$	$128/105$	$-64/63$
$p=8$	0.996084	0.999703	1.000080	1.000068
$p=7$	0.995804	0.999439	0.999819	0.999805
$p=6$	0.995966	0.999646	1.000032	1.000016
$p=5$	0.997801	1.001348	1.001692	1.001663
$p=4$	0.994830	0.998490	0.998890	0.998882
$p=3$	0.989424	0.995263	0.996286	0.996391

Table 6. *Values of* $J[R]/J_{\rm ex}$ *, for Case 5 with* (BC_2) *at* $R = 0.02$ *using different* p *-FEM.*

Cb Errors due to Gaussian Quadrature

The second source of numerical error is due to the Gauss quadrature used to evaluate the integral $J[R]$. One needs to evaluate a double integral over θ and x_3 . The Gauss quadrature order n_G controls the numerical error in this case. In order to evaluate the influence of the quadrature order, $J[R]$ was computed with various quadrature orders. The results presented in Table 7 are the values of $J[R]/J_{\rm ex}$ for Case 5 with (BC_2) again, using the quasi-dual functions $K_0^{(\alpha_1)}$ to $K_3^{(\alpha_1)}$. The values of $J[R]/J_{\rm ex}$ are not influenced by the quadrature computation even at low order as 10.

$B(x_3)$	1	(x_3-1)	$(x_3-1)^2$	$(x_3-1)^3$
$J_{\rm ex}$	$8/3$	$-8/5$	$128/105$	$-64/63$
$n_G=10$	0.996092	0.999705	1.000079	1.000064
$n_G=15$	0.996084	0.999703	1.000080	1.000068
$n_G=32$	0.996085	0.999701	1.000077	1.000064

Table 7. *Values of* $J[R]/J_{\rm ex}$ *, for Case 5 with* (BC_2) *at* $R=0.02$ *using different* n_G *.*

References

[1] M. Abramowitz and A. Stegun. *Handbook of mathematical functions with formulas, graphs and mathematical tables*. Nat. Bureau of Standards, Applied Mathematics Series, 1964.

[2] I. Babuška, T. Von-Petersdorff, and B. Andersson. Numerical treatment of vertex singularities and intensity factors for mixed boundary value problems for the Laplace equation in R^3 . *SIAM Jour. Numer. Anal.*, 31(5):1265–1288, 1994.

[3] A. Beagles and A.-M. Sändig. Singularities of rotationally symmetric solutions of boundary value problems for the Lamé equations. *ZAMM - Z. Angew. Math. Mech.*, 71:423–431, 1991.

[4] H. Blum and M. Dobrowolski. On finite element methods for elliptic equations on domains with corners. *Computing*, 28:53–63, 1982.

[5] M. Chiarelli and A. Frediani. A computation of the 3-dimensional J-integral for elastic-materials with a view to applications in fracture-mechanics. *Engrg. Frac. Mech.*, 44(5):763–788, 1993.

[6] M. Costabel and M. Dauge. General edge asymptotics of solution of second order elliptic boundary value problems I & II. *Proc. Royal Soc. Edinburgh*, 123A:109–184, 1993.

[7] M. Costabel, M. Dauge, and Y. Lafranche. Fast semi-analytic computation of elastic edge singularities. *Computer Meth. Appl. Mech. Engrg.*, 190:2111–2134, 2001.

[8] M. Costabel, M. Dauge, and Z. Yosibash. A quasidual function method for extracting edge stress intensity functions. *SIAM Jour. Math. Anal.*, 35(5):1177–1202, 2004.

[9] M. Dauge. *Elliptic boundary value problems in corner domains - smoothness and asymptotics of solutions*. Lecture notes in Mathematics 1341, Springer-Verlag, Heidelberg, 1988.

[10] M. Dauge. Corner – Edge Asymptotics in Polyhedral Domains. URL address — `http://perso.univ-rennes1.fr/monique.dauge/publis/corneredge.html`, 2000.

[11] G. Dhondt, A. Chergui, and FG. Buchholz. Computational fracture analysis of different specimens regarding 3D and mode coupling effects. *Engrg. Frac. Mech.*, 68(4):383–401, 2001.

[12] P. Grisvard. *Elliptic problems in nonsmooth domains*. Pitman Publishing, England, 1985.

[13] V.G. Maz'ya and B.A. Plamenevskii. L^p estimates of solutions of elliptic boundary value problems in a domain with edges. *Trans. Moscow Math. Soc.*, 1:49–97, 1980.

[14] O. Huber, J. Nickel, and G. Kuhn. On the decomposition of the J-integral for 3D crack problems. *Int. Jour. Fracture*, 64(4):339–348, 1993.

[15] G. Meda, T.W. Messner, G.B. Sinclair, and J.S. Solecki. Path-independent H integrals for three-dimensional fracture mechanics. *Int. Jour. Fracture*, 94(3):217–234, 1998.

[16] R.H. Rigby and M.H. Aliabadi. Decomposition of the mixed-mode J integral - revisited. *Int. Jour. Solids and Structures*, 35(17):2073–2099, 1998.

[17] Z. Yosibash, R. Actis, and B. Szabó. Extracting edge flux intensity functions for the Laplacian. *Int. Jour. Numer. Meth. Engrg.*, 53(1):225–242, 2002.

[18] Z. Yosibash, A. Bussiba, and I. Gilad. Failure criteria for brittle elastic materials. *Int. Jour. Fracture*, 125(3-4):307–333, 2004.